molecules

MDPI

Review

Recent Advances in Two-Dimensional MXene-Based Electrochemical Biosensors for Sweat Analysis

Selvaganapathy Ganesan [1,2], Kalaipriya Ramajayam [1,2], Thangavelu Kokulnathan [3,*] and Arunkumar Palaniappan [2,*]

[1] Department of Chemistry, School of Advanced Sciences, Vellore Institute of Technology, Vellore 632014, Tamil Nadu, India; selvaganapathy.g@vit.ac.in (S.G.); kalaipriya.r@vit.ac.in (K.R.)
[2] Centre for Biomaterials, Cellular and Molecular Theranostics, Vellore Institute of Technology, Vellore 632014, Tamil Nadu, India
[3] Department of Electro-Optical Engineering, National Taipei University of Technology, Taipei 106, Taiwan
* Correspondence: kokul49@mail.ntut.edu.tw (T.K.); arunkumar.p@vit.ac.in (A.P.)

Abstract: Sweat, a biofluid secreted naturally from the eccrine glands of the human body, is rich in several electrolytes, metabolites, biomolecules, and even xenobiotics that enter the body through other means. Recent studies indicate a high correlation between the analytes' concentrations in the sweat and the blood, opening up sweat as a medium for disease diagnosis and other general health monitoring applications. However, low concentration of analytes in sweat is a significant limitation, requiring high-performing sensors for this application. Electrochemical sensors, due to their high sensitivity, low cost, and miniaturization, play a crucial role in realizing the potential of sweat as a key sensing medium. MXenes, recently developed anisotropic two-dimensional atomic-layered nanomaterials composed of early transition metal carbides or nitrides, are currently being explored as a material of choice for electrochemical sensors. Their large surface area, tunable electrical properties, excellent mechanical strength, good dispersibility, and biocompatibility make them attractive for bio-electrochemical sensing platforms. This review presents the recent progress made in MXene-based bio-electrochemical sensors such as wearable, implantable, and microfluidic sensors and their applications in disease diagnosis and developing point-of-care sensing platforms. Finally, the paper discusses the challenges and limitations of MXenes as a material of choice in bio-electrochemical sensors and future perspectives on this exciting material for sweat-sensing applications.

Keywords: point-of-care; diagnostic; wearable sensor; glucose monitoring

check for updates

Citation: Ganesan, S.; Ramajayam, K.; Kokulnathan, T.; Palaniappan, A. Recent Advances in Two-Dimensional MXene-Based Electrochemical Biosensors for Sweat Analysis. *Molecules* **2023**, *28*, 4617. https://doi.org/10.3390/molecules28124617

Academic Editor: Antonella Curulli

Received: 8 May 2023
Revised: 3 June 2023
Accepted: 5 June 2023
Published: 7 June 2023

Copyright: © 2023 by the authors. Licensee MDPI, Basel, Switzerland. This article is an open access article distributed under the terms and conditions of the Creative Commons Attribution (CC BY) license (https://creativecommons.org/licenses/by/4.0/).

1. Introduction

The current healthcare system is taking a transition from a conventional approach, where patients visit a healthcare professional for any medical aid after developing the disease or its symptoms, towards more sophisticated continuous monitoring of vital biomarkers and then informing patients (sometimes by healthcare professionals remotely) of any deviation from the normal level. This enables early detection of any deviation from the level of the normal biomarker and brings in new possibilities for the prevention of disease that are not possible through the conventional system. This requires highly specific and sensitive biosensing platforms for precisely and continuously monitoring the biomarkers. The electrochemical-based wearable sensors are currently being explored on this line and are found to be an excellent sensing platform to address the above challenges [1–3]. Thus, wearable electrochemical biosensors can provide continuous, instantaneous data on patients' physiologies via dynamic, non-invasive measures of biomarkers in biofluids without causing discomfort to the wearing individuals [4–8]. In recent years, the growth of wearable electronic technologies that can precisely quantify vital responses such as body temperature, blood pressure, blood sugar level, and heart rate, aiding in depicting and monitoring the

individual's health conditions, has accelerated [3,9]. However, these biological parameters cannot provide complete information on the human body's robust biochemical and metabolic functions [10]. So, biofluids such as tears, saliva, and sweat are of massive interest to biosensors researchers for their ease of sampling and their demonstrated capabilities to provide continuous and instantaneous monitoring of vital biomarkers and parameters, which could give insights into the subject's physiology in a non-invasive manner [11–16]. Compared to other biofluids, sweat is high in several essential analytes such as glucose [17], lactate [18], cortisol [18], uric acid [19], interleukin [20], ammonium [21], sodium [22], potassium [23], calcium [24], iron [25], and zinc [26]. They provide critical physiological information about the human body and are closely intertwined with capillaries and nerve fibers, offering an immense advantage for biosensing applications. Moreover, wearable analytes monitoring technologies at sweat production sites open a huge possibility of autonomous, continuous, and instantaneous sensing of vital analytes present in sweat.

The first work on wearable electrochemical sensors for real-time monitoring of sweat lactate was developed by Jia et al. [27]. Further, many researchers have executed the monitoring of metabolites, electrolytes, drugs, and trace elements present in sweat. Electrochemical sensing is a familiar and deep-rooted method for detecting sweat analytes that is extensively used in wearable sensing platforms and often used in clinical diagnostics due to its simplicity, portability, high performance, and low cost [28–30]. Some recent technological developments are steering the sophistication of wearable sweat sensors based on electrochemical methods. A complete unified multiplexed sensing device for simultaneous monitoring of multiple analytes makes the system more practical. It offers a versatile wearable electrochemical biosensing platform for large-scale clinical diagnostics and physiological understandings [31–33]. Thus, the performance and effectiveness of the wearable biosensor rely heavily on the properties of materials used to make the device.

Some of the most common materials used in biosensors include and are not limited to the following: graphene and its derivatives [34,35], transition metal nanoparticles [36–39], transitional metal dichalcogenides [40,41], gold nanoparticles [42,43], silver nanoparticles [44,45], and very recently, transition metal carbides/nitrides, called as MXenes [46]. Because of their excellent multifaceted characteristics including high surface area, size control, tunable electronic and mechanical properties, high biocompatibility, exceptional sensitivity, specificity, and low detection limit (LOD), MXenes are currently being explored heavily for fabricating biosensors compared to other nanomaterials. MXenes are a class of 2D inorganic nanomaterials with few-atom thicknesses made of layered transition carbides, nitrides, and carbonitrides [47–49]. They are typically exfoliated by etching of the A layer from the MAX phase, specifically [50]. The general formula of an MXene is $M_{n+1}X_nT_x$, where M represents the early transition metals, X is for carbon or nitrogen, T is for surface functional groups (–OH, –F, =O), and n represents an integer.

This review systematically summarizes recent breakthroughs in MXene-based electrochemical biosensors for sweat analytes. We review and discuss various synthesis methods for MXenes, their surface chemistry, and functionalization strategies in sensor applications. The advantages and importance of sweat analytes in continuously monitoring human physiology and disease conditions are also highlighted. Finally, we also discuss various MXene-based wearable biosensors for vital analytes in sweat. Most importantly, this review sheds light on future scopes and recommendations for researchers working on MXenes for electrochemical biosensor applications.

2. Advantages of Sweat as an Analyte in Biosensing

In the current healthcare systems, blood serum is considered as the gold standard to determine the concentration of analytes in most cases [51,52]. However, the invasive methods of sampling blood from patients produce more impediments, particularly for hemophobic patients, new-borns, and elderly persons. Urine is also a biofluid widely used as clinical samples but has some limitations for autonomous and continuous monitoring [53]. Saliva is another biofluid that contains many biomarkers, including enzymes, hormones, antibodies,

and antimicrobial agents, which can precisely provide details on the molecular state of human physiology [54]. However, saliva monitoring also has specific drawbacks, such as saliva in the mouth containing many impurities and food particles, which could affect the precision of results. Tears, another biofluid, contain enzymes, proteins, lipids, and certain salts, which can reflect the conditions and disease in the eyes and others [55]. Unfortunately, the present tear sample collection protocols produce reflex tears and eye irritation, which can also affect the results of sensor analysis.

In contrast to other biofluids such as blood, urine, saliva, and tears, sweat has a massive advantage in biosensing applications. Sweat regulates heat balance in the body and plays crucial physiological roles including immune defense, thermoregulation, moisturization, and pH balance [56,57]. Thus, sweat contains several biomarkers that can provide the complete physiological status of the body at the molecular level [58,59]. The sweat glands in the body secrete the sweat. Thus, sweat analytes can be collected in a non-invasive manner from different body parts and are optimal for continuous monitoring. The average density of sweat glands in the body and the approximate range of analytes' concentrations in the sweat fluid are shown in Figure 1a,b [60]. Key analytes in human sweat and associated health conditions are shown in Table 1.

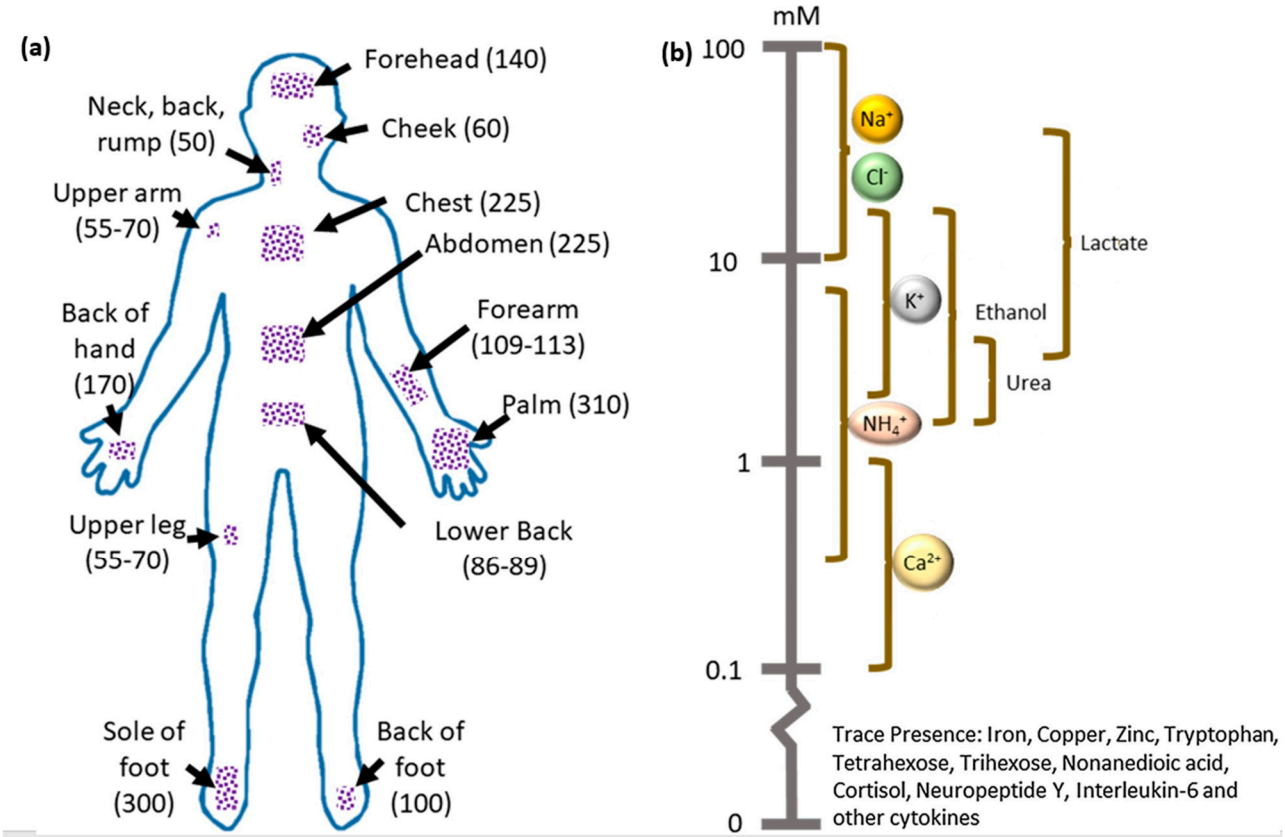


Figure 1. (**a**) Schematic representation of the average density of sweat glands in the different parts of the human body (glands/cm^2). (**b**) Approximate range of analytes' concentrations present in the sweat. Reproduced with permission from Ref. [60]. Copyright 2019 Elsevier.

Table 1. Key analytes present in human sweat and associated with health issues.

Analytes	Health Condition	Refs.
Iron	Sports anemia	[25]
Glucose	Key analyte for diabetic conditions	[61,62]
Lactate	Analytes accumulated during a transition from aerobic to anaerobic conditions.	[63,64]
Uric acid	Gout, Renal dysfunction	[65]
Zinc (Zn^{2+})	Immune system-induced muscle damage	[66,67]
Copper (Cu^{2+})	Rheumatoid arthritis, Cirrhosis of liver	[67,68]
Interleukin 6	Proinflammatory cytokines, markers for certain cancers, and inflammation	[69,70]
Cortisol	Stress	[71]
Neuropeptide Y	Stress	[72]
pH	Wound healing, Skin diseases—pathogenic	[73]
Sodium (Na^{+})	Dehydration, Electrolyte imbalance, Hyponatremia	[74,75]
Cl^{-}	Cystic fibrosis, Dehydration	[76]
Potassium (K^{+})	Hypokalaemia, Muscle cramps	[77]
Calcium (Ca^{2+})	Renal failure, Acid-base balance disorder, Myeloma	[78]
Ammonium (NH_4^{+})	The shift from aerobic to anaerobic conditions	[79,80]

3. MXenes–A Material of Choice for Biosensors

In contrast to metal nanoparticles- and graphene derivative-based biosensors, MXenes have gained much attention in developing biosensors due to their excellent biocompatibility and high electrical conductivity properties. A suitable sensor possesses high specificity, sensitivity, LOD, quick response, and a wide operating range. In addition, it also needs to be less expensive not only in lab-scale use, but also while scaling up. MXenes have all/most of these very important properties in the development of biosensors [81–84].

3.1. Synthesis Strategies of MXenes

MXenes, a new class of 2D anisotropic nanomaterial, have significantly improved from their first discovery in 2011 ($Ti_3C_2T_x$) by the selective etching of the MAX phase precursor Ti_3AlC_2 [85]. Typically, MXenes are developed by removing the A layer from their MAX phase via specific etching. The synthetic methods of MXenes can be classified into two types: the top-down approach and the bottom-up approach. The top-down approach involves the direct exfoliation of the A layer, while the bottom-up approach is based on 2D ordered growth from atoms/molecules. Both the methods are discussed in detail in the below sections.

3.1.1. Top–Down Approach

The top–down approach involves the direct exfoliation of the bulk parent MAX phase material with its original integrity retained. These exfoliation processes are typically carried out using chemical and mechanical methods. The top-down approach can be further classified based on the type of precursors used, the delamination process, and the etchants involved in the reaction. The following section describes these methods in more detail.

Based on Precursors

Based on the precursors selected, the preparation strategy of MXenes is classified into MAX-phase and non-MAX-phase methods. In the MAX phase-based preparation method, the A layer is eliminated by using specific selective etchants with optimized concentrations and time intervals, followed by filtration and sonication to obtain few-layered 2D nanosheets. A typical example of this method is the elimination of the A layer from the MAX phase (Ti_3AlC_2) to form $Ti_3C_2T_x$ MXene by Naguib et al. (Figure 2a), with hydrofluoric acid (HF) as an etchant in room temperature conditions [85].

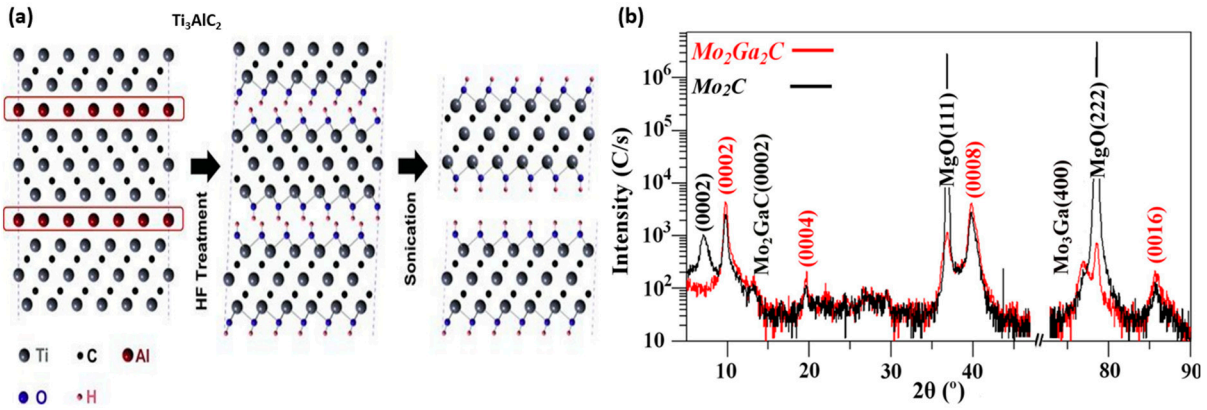


Figure 2. (**a**) Schematic illustration of the synthesis process of Ti_3AlC_2. Reproduced with permission from Ref. [85] Copyright 2011 John Wiley and Sons. (**b**) X-ray diffraction pattern of Mo_2Ga_2C film before and after HF etching. Reproduced with permission from Ref. [86]. Copyright 2015 Elsevier.

Non-MAX phase-based synthesis was obtained from the selective etching of the gallium (Ga) layer from the Mo_2Ga_2C with 50% concentrated HF acid to form Mo_2CT_x MXene [86]. In contrast to the known MAX phase formula, the non-MAX phase method of prepared Mo_2CT_x MXene consists of two A layers of Ga stacked between the Mo_2C layers. To confirm perfectly etched treatment, the X-ray diffraction patterns of Mo_2CT_x and Mo_2Ga_2C before and after etching were compared (Figure 2b), in which there was a significant reduction in the peak intensity of Mo_2C, which confirms the Ga phase was dissolved during the etching process.

Based on Delamination

In general, synthesizing single-layered MXenes requires further processing steps on the multi-layered MXenes, called delamination. The delamination of multi-layered MXenes can be by the intercalation method or through mechanical exfoliation. It was reported that mechanical exfoliation is ineffective because the interlayer interactions in MXenes produced by this method are highly tacky (the interlayer interaction in the MXene is two- to six-folds stronger than that present in graphite and bulk MoS_2 [87]). Moreover, the sonication time also affects the lamellar structure, decreases MXene sheet size, and produces defects in the structure [88–90].

In the case of the intercalation method, intercalants are introduced to reduce the interlayer spacing, weaken the interaction between the MXene layers, and facilitate the formation of individual nanosheets. This dramatically improves the surface area and abundant surface terminations directly associated with the MXene's electrically conductive properties. The intercalants widely used for intercalations of the MXene are classified into two types: ionic aqueous solutions that include metal hydroxides or halide salts as aqueous solutions [91,92] and organic intercalants such as dimethyl sulfoxide (DMSO) [93], tetrabutylammonium hydroxide (TBAOH) [94], tetra propylammonium hydroxide (TPAOH) [95], isopropyl amine [96], n-butyllithium [97], and bovine serum albumin (BSA) [98].

Based on Etchants

HF etching

In the HF etching-based MXene synthesis method, the layered MAX phase is stirred with HF aqueous solution at room temperature with specified concentration and time. Here, the multi-layered MXene is produced by an etched A layer from the MAX phase, and M-A bonds are replaced by the weak intercalations of T_x termination such as (–OH, –F, =O) on the surface of the multi-layered MXene. In agreement with numerous studies in recent times, several etching parameters such as temperature, time, and concentration of etchant play a deterministic role in the standard of the prepared MXene nanosheets. Kumar et al. demonstrated the effectiveness of $Ti_3C_2T_x$ MXene etched at elevated temperatures for a binder-free supercapacitor application (Figure 3a–d) [99].

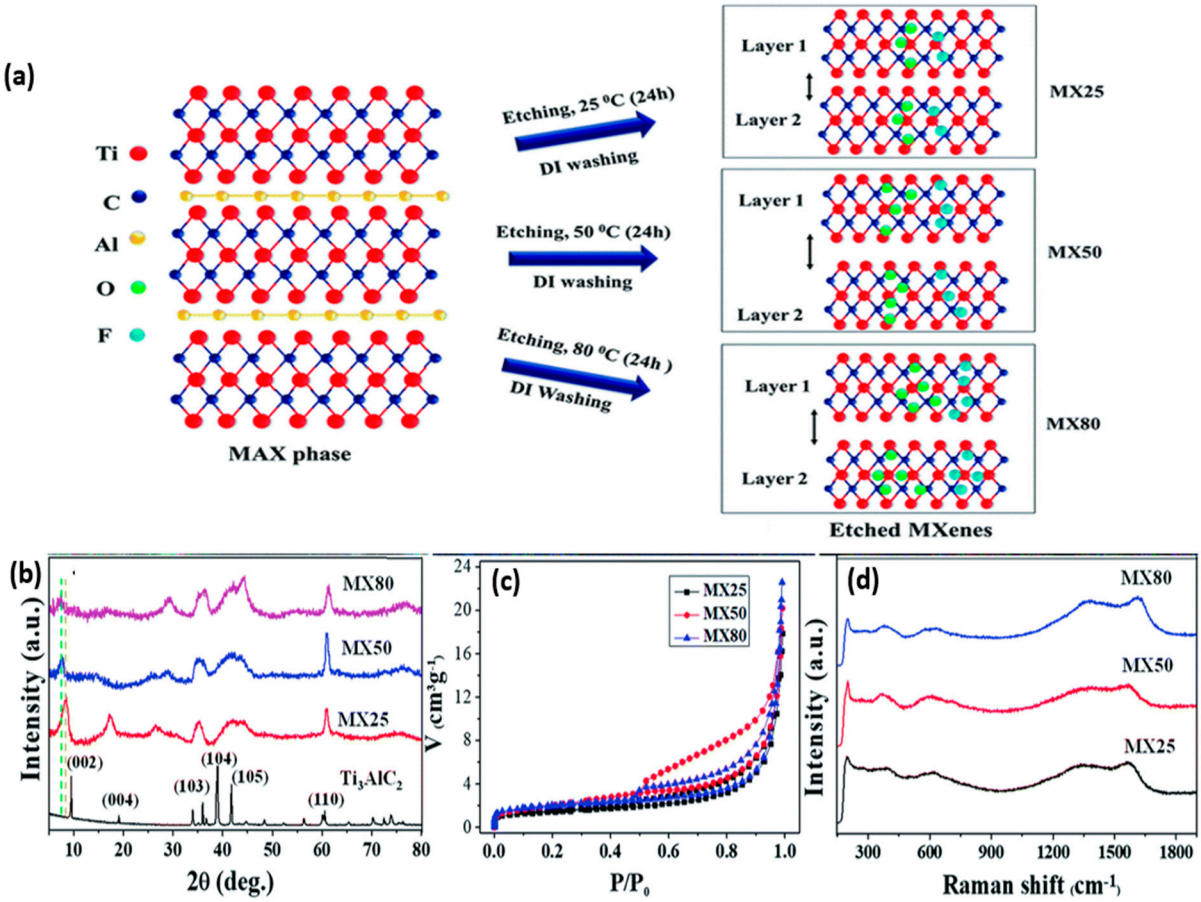


Figure 3. (**a**) Schematic representation of the etching mechanism at elevated temperature and their high exfoliation. (**b**) XRD pattern of exfoliated material at different temperatures and reduced intensity at high–temperature etching of MX80 indicates deterioration of crystallinity. (**c**) BET isotherm studies confirm the increase in surface area with high–temperature etching. (**d**) Raman spectra of exfoliated MXene at different temperatures were high–intensity peaks observed for MX80, indicating the defects introduced at high–temperature etching. Reproduced from Ref. [99] with permission from the Royal Society of Chemistry.

Non–HF etching

Even though HF is extensively and effectively utilized to prepare MXenes from the MAX phase, it is highly corrosive and hazardous to humans and the environment [100–102]. A trace amount of HF remaining in the MXene sample will harm the composite preparation and biological studies carried out further. Thus, the etching of MXenes by non-HF-based solvents is also extensively studied. The alternative etchants used for etching MXenes are weak acids

and environmentally friendly bifluorides such as sodium bifluoride ($NaHF_2$), ammonium bifluoride (NH_4HF_2), and potassium bifluoride (KHF_2). Feng et al. demonstrated the synthesis of $Ti_3C_2T_x$ MXene from the Ti_3AlC_2 MAX phase with bi-fluoride in a single-stage process. They found that the NH_4^+, Na^+, or K^+ ions enter the interlayer spacing of the MXene and enlarge the interplanar spacing and delamination efficiency [103].

In comparison to carbide-based MXenes, the Al layer is strongly bonded in the nitride-based MXene. Thus, more energy is required to remove the A layer from the nitride-based MXene. Moreover, the nitride-based MXene is less stable and might be able to dissolve in HF [104,105]. To overcome this issue, molten fluoride is used with the support of high-temperature heating to remove the A layer from the nitride-based MXene. Urbankowski et al. heated the Ti_4AlN_3 powder at 550 degrees for 30 min under an argon atmosphere with molten fluoride, where the free F^- ions were active enough to etch the Al layer from the nitride MXene MAX phases [106]. Studies revealed that the etchants are an essential determinant in the surface termination of the synthesized MXene. The fluorine-based etchants increase the percentage of F content in the surface terminations. Therefore, further modifications are needed for particular applications such as biomedical and sensors [107,108].

3.1.2. Bottom–Up Approach

MXenes can also be synthesized by crystal growth methods using a small organic or inorganic molecule as the precursor. The bottom-up approaches enable precise manipulation of the size of the MXene sheet, geometry, and the surface termination groups in the MXene, which are impossible using top-down approaches [109–112]. However, compared to the top-down approach of MXene preparation, only a few studies have been performed with the bottom-up approach, perhaps due to the difficulty in the bottom-up approach to build atom-by-atom the MXene's complex structure and multi-component atomic-thick layer. Moreover, the mechanisms of interaction between the layers are still not clear.

Hong et al. demonstrated the preparation of Mo_2N MXene sheets by the chemical vapor deposition (CVD) method with NH_3 as the source in the temperature range of 1080 °C [112]. Similarly, Ren et al., 2015 developed ultrathin α-Mo_2CT_x crystals with excellent stability and defect free by CVD [113]. Buke et al. reported a detailed study on the effect of temperature, time, and copper layer thickness in the preparation of an MXene by the CVD method. In addition, they also found that Mo_2C MXene crystals formed on the graphene sheets are thinner than those formed on the copper sheets [114]. In continuation to the CVD method, pulse laser deposition (PLD) and salt template methods were also investigated for the preparation of MXenes through a bottom-up approach [115,116].

3.2. Properties of Mxenes

MXenes have already proven their steadfast importance in multiple applications such as catalysis [117]; sensors (optical [118,119]; electrochemical [120–126]; surface-enhanced Raman scattering [127,128]; biomedical applications [129,130]; electromagnetic shielding [131–133]; and energy storage [134,135]. This success is significantly due to its unique properties, such as high young's modulus [136,137], adjustable band gap [138], and thermal and electrical conductivity [139]. Comparison of fundamental properties of nanomaterials are shown in Table 2.

3.2.1. Electrical Properties

Similar to the MAX phase, a pristine MXene is all-metallic. Thus, the research has been focused on enhancing the conductivity nature of MXenes by engineering their surface chemistry [140,141]. The prepared MXene using etchants leaves a surface termination group (–OH, –F, =O) which will bond to the metal atom in the MXene. Based on the experimental and theoretical studies, a few reports showed that some termination groups may affect the conductive property of the MXene [142–144] and electron mobility [145–147]. Yan et al. demonstrated an alkaline-treated MXene for humidity sensors, where they showed similar effects of –OH and –O termination groups in enhancing the electrochemical capacitance

and sensor properties [107,148,149]. Pandey et al. investigated the electronic properties of $M_nC_{n-1}O_2$ MXenes (M = Ti, W, Ta, Hf, Sc Mo, Nb, Cr, Zr, Y, Mn, V) [150], in which they found that oxygen-terminated MXenes are favorable for many applications.

Table 2. Comparison of fundamental properties of nanomaterials.

Nanomaterials	Conductivity (S/cm)	Surface Area (m^2 g^{-1})	Biocompatibility	References
Graphene	2700	450	Biocompatible	[151,152]
Single-walled carbon nanotubes	10^2 to 10^6	600	Under debate	[153–155]
Multiwalled carbon nanotubes	10^3 to 10^5	122	Under debate	[153–155]
Hexagonal boron nitride	Insulator	150–550	Depends on the shape and size	[156,157]
MnO_2	10^{-5} to 10^{-6}	257.5	Biocompatible	[158–160]
MoS_2	10^{-4}	8.6	Biocompatible	[161–163]
MXene-Ti_3C_2	15100	93.6	Biocompatible	[164–168]

3.2.2. Biocompatibility of MXenes

The principal mechanisms of nanomaterials' toxicity could be one of the following: (1) damage to cells, (2) genotoxicity, (3) slow clearance in the renal pathway and accumulation in the organs, and (4) specific toxicity to the neural and reproductive system. Thus, an extensive biological safety evaluation is required to understand all the possible interactions between the nanomaterials and the physiological systems. MXenes, due to their high surface area and hydrophilicity, provide a suitable matrix for fabricating wearable biosensors [169]. Some preliminary results on MXene cytocompatibility and biocompatibility are already explored in the literature. Ti_3C_2 MXene is the most commonly investigated system in biomedical applications [166,170–172]. Liu et al. developed Ti_3C_2 MXene nanosheets for theranostics applications. They revealed that the MXene nanosheets passed in the bloodstream are excreted through human urine via the renal clearance pathway or accumulated in the tumor tissue due to the enhanced permeability and retention effect (EPR). In this study, the Ti_3C_2 nanosheets' biosafety and biocompatibility are confirmed by the absence of significant weight loss and the absence of necrotic process. Han et al. investigated the in vivo biocompatibility of Ti_3C_2 MXene by administering the MXene to mice at elevated dosages (6.25, 12.5, 25, and 50 mg/kg), which resulted in excellent in vivo biocompatibility at 25 mg/kg [173]. In a similar study, Zong et al. developed a Ti_3C_2-GdW10 nanocomposite for cancer theranostics application. The in vivo biocompatibility studies concluded that up to 50 mg/kg of Ti_3C_2-GdW10 nanocomposite was biocompatible using female Kunming mice [174]. Similar results have been reported for systematic cytocompatibility and biocompatibility of tantalum carbide-based MXene Ta_4C_3 [171,175] and niobium carbide MXene Nb_2C [176,177].

4. MXene-Based Electrochemical Sweat Sensors

Due to the fascinating physiochemical properties of MXenes and their composites, they have gained strong attention in biosensing with their excellent sensitivity, specificity, LOD, mechanical properties, and biocompatibility [136,144,178,179].

4.1. Glucose Sensing

Peng et al. developed a Pt/Ti_3C_2 MXene-based wearable, flexible non-enzymatic electrochemical biosensor for continuous monitoring of glucose in sweat [180]. Figure 4a–c illustrates the fabrication process of the sensor, microfluidic patch, and integration of the flexible sensor to the prepared patch. Figure 4d–f shows the conceptual scheme of the sensor for glucose detection, the cross-sectional view of the sensor on the skin, and the oxidation mechanism of the material and analyte. Figure 4g,h shows the electrochemical

reaction mechanism of Pt/Ti_3C_2 coated on a glassy carbon electrode (GCE) and fabricated flexible sensor. This system offers a LOD of 29.15 µmol L^{-1} with a correlation coefficient of 0.9793.

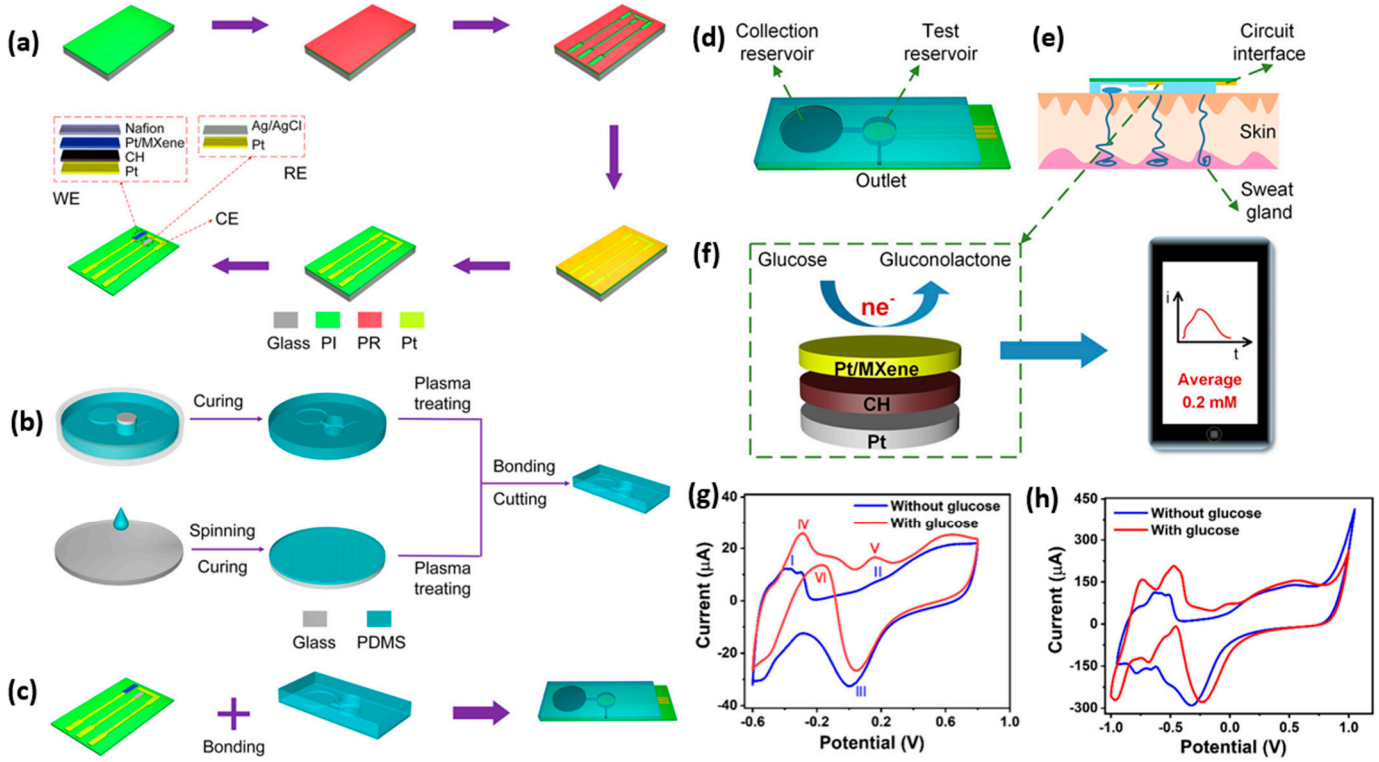


Figure 4. (**a**) Schematics show the flexible sensor's fabrication process. (**b**) The preparation process of the microfluidic patch. (**c**) Integration of MXene–based sensor to microfluidic patch. (**d**) Schematic overview of the proposed flexible wearable sensor. (**e**) Cross–sectional view of the sensor on the skin. (**f**) The electrochemical oxidation reaction of glucose on the MXene. (**g**) CV response of Pt/Ti_3C_2 MXene coated on GCE. (**h**) CV response of Pt/Ti_3C_2–fabricated flexible wearable sensor. The figure is reproduced with permission from [180]. The copyright year is 2023 American Chemical Society.

In another work by Park et al., 2022, a butterfly-inspired hybrid epidermal biosensing (*bi*-HEB) patch, made with carbon $Ti_3C_2T_x$ MXene-based nanocomposite, was developed for simultaneous monitoring of glucose and electrocardiograms (ECGs) in human subjects while performing indoor physical activities [73]. This system demonstrated excellent sensitivity of 100.85 µAmM^{-1} cm^{-2} within physiological levels (0.003−1.5 mM). Moreover, variations in pH and temperature from on-body sweat monitoring are calibrated. Figure 5a–c is a detailed schematic overview of *bi*-HEB patch fabrication. Feng et al. demonstrated a 3D porous $Ti_3C_2T_x$/graphene/AuNP composite electrochemical biosensor for quick, responsive glucose detection. This system has a LOD of 2 µM in a concise time of fewer than 3 s with a sensitivity of 169.49 µA/(mM·cm^2) in the range of 2 µM–0.4 mM concentration of glucose [181]. Hosseini et al. fabricated a Ti_3C_2/nickel-samarium-layered double hydroxide for enzyme-free real-time glucose detection. The glucose sensing was investigated with the DPV method, resulting in a LOD value of 0.24 µM and a linear range from 0.001 to 0.1 mM and 0.25–7.5 Mm [182].

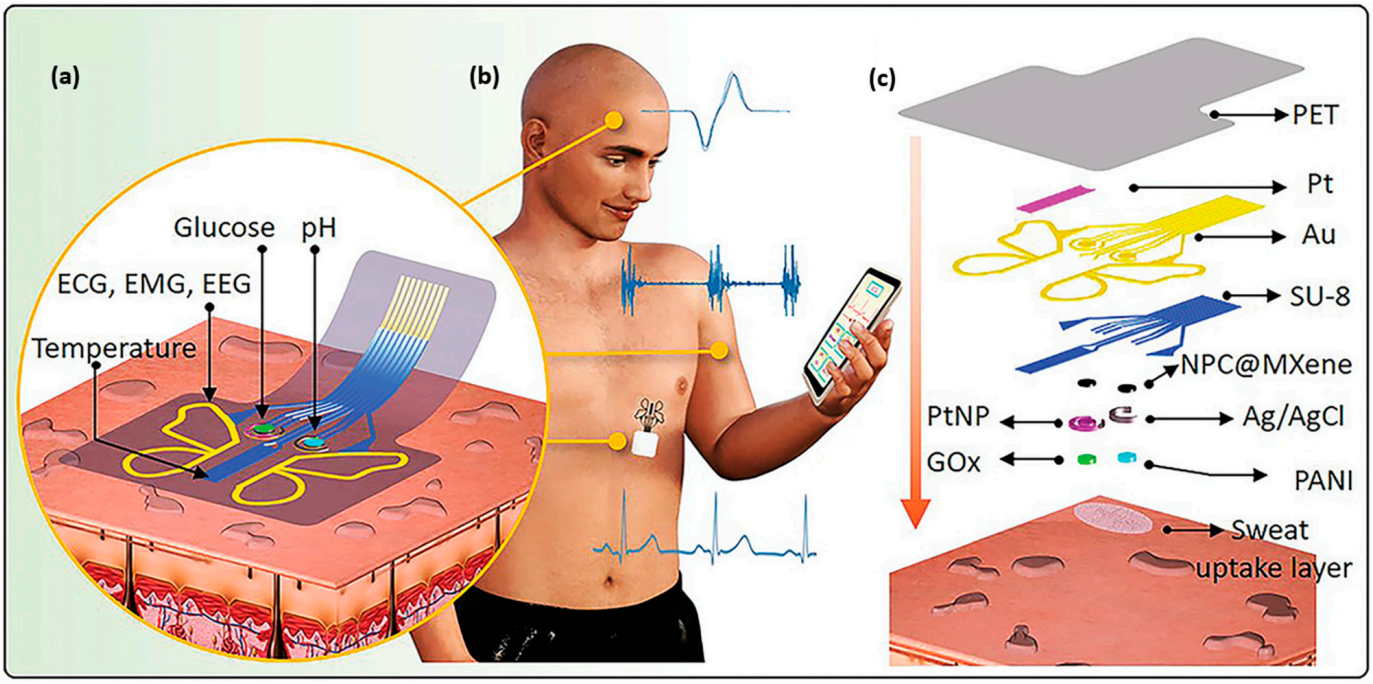


Figure 5. (**a**) Schematic illustration of layer-by-layer assembled multiplexed electrochemical sensor mounted on the skin containing various analyte-templated patterns designed on thin polyethylene terephthalate (PET) substrate. (**b**) *bi*-HEB patch mounted at the chest to monitor sweat glucose, temperature, and pH simultaneously. (**c**) Schematic representation of layer-by-layer fabrication process of the *bi*-HEB patch from top to bottom. Reproduced with permission from Ref. [73]. Copyright 2022 John Wiley and Sons.

Li et al. demonstrated a highly integrated wearable sensing paper (HIWSP) for electrochemical analysis of glucose and lactate from sweat [183]. This paper composition contains hydrophobic-layered protecting wax, a hydrophilic layer for sweat diffusion, and a $Ti_3C_2T_x$ MXene/methylene blue composite. This sensor had a sensitivity of 2.4 nA μM^{-1} and 0.49 μA mM^{-1} for the simultaneous detection of glucose and lactate, respectively. In another work, Lei et al. fabricated a high-performing wearable biosensor for in vitro perspiration analysis [184]. This multifunctional biosensor is designed by incorporating $Ti_3C_2T_x$ MXene and Persian blue composite for durable and sensitive monitoring of glucose and lactate in sweat. Figure 6a–i illustrates the real-time monitoring of wearable patches indicating pH, glucose, and lactate. Magesh et al. fabricated a palladium hydroxide integrated $Ti_3C_2T_x$ MXene composite electrode to detect nicotine analyte in human sweat. This analysis was performed with the help of CV and amperometric studies and exhibited a LOD value of 27 nM with a sensitivity of 0.286 μA μM^{-1} cm^{-2} [185].

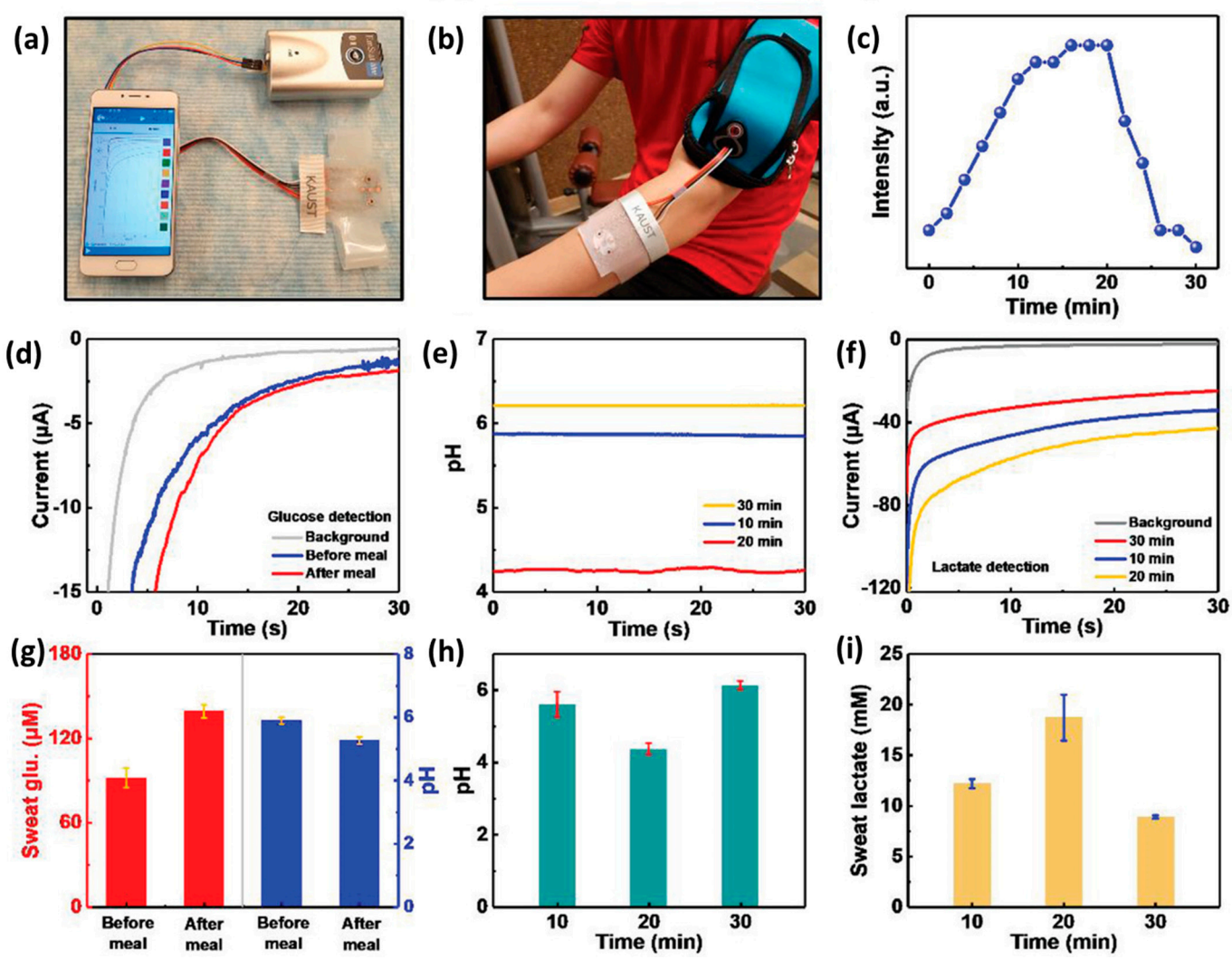


Figure 6. (**a**) Photograph of wearable sweat monitoring patch connected to a portable electrochemical analyzer that supplies power and can wirelessly communicate the body's status with mobile phones via Bluetooth. (**b**) Skin–attached wearable sweat sensor. (**c**) Graphical data of on–body test cycling resistance profile. (**d**) Chronoamperometric response of pH changes and glucose sensor before and after a meal. (**e**) pH response at different times during exercise. (**f**) The electrochemical response of lactate sensor at different times during exercise. (**g**) Comparison of pH level and glucose after a meal with three different sensors. (**h**) Comparison of pH levels at different times during exercise. (**i**) Comparison of lactate sensor responses at different exercise times with different lactate sensors. Reproduced with permission from Ref. [184]. Copyright 2019 John Wiley and Sons.

$Ti_3C_2T_x$ MXene nanoflakes decorated ZnO tetrapods (ZnO TPs), a graphene oxide composite, and a skin-attachable enzymatic electrothermal glucose sensor was fabricated by Myndrul et al. [186]. This system showed a LOD of 17 μM with a broad linear detection range of 0.05–0.7 mM for detecting glucose from human sweat. Figure 7a–d shows stretchable electrodes at various strains, glucose sensing performance at applied strain (artificial sweat), skin-attachable sensor performance, and current density changes in the fabricated sensors on volunteer sweet consumption for glucose monitoring.

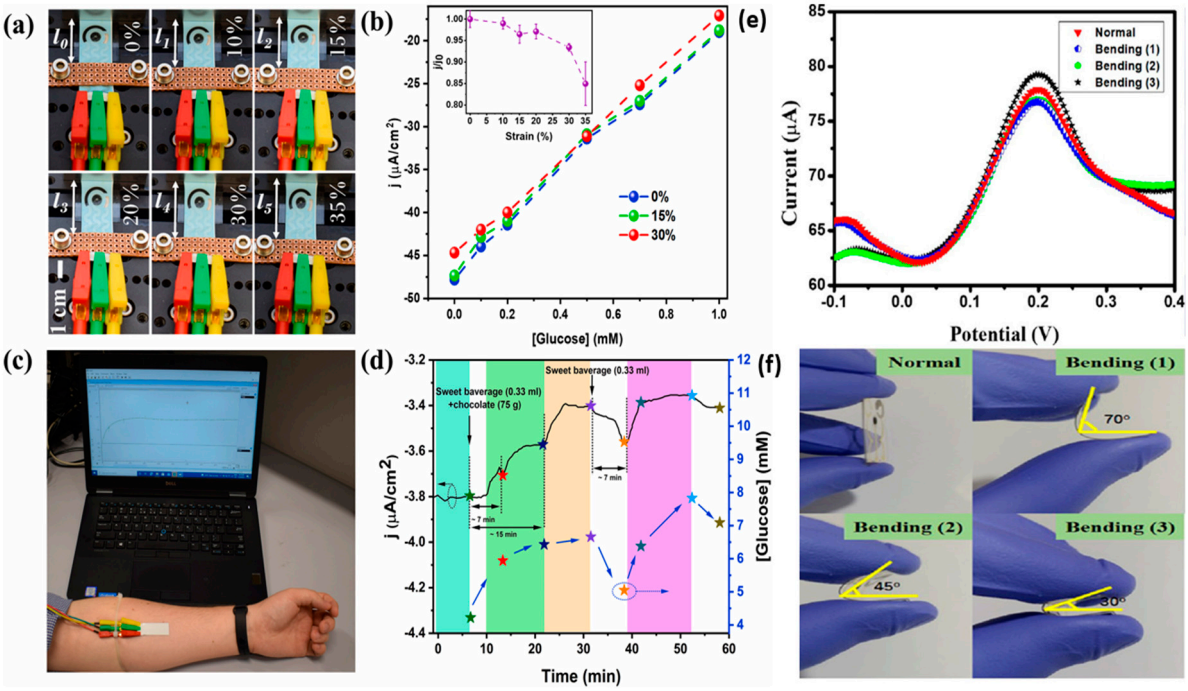


Figure 7. (**a**) Picture of flexible MXene/ZnO TPs/Gox composite electrode at strain range of 0–35%. (**b**) Working performance of fabricated sensor at applied strains (electrode current density *vs* applied strains) graph. (**c**) Photograph of skin–attachable sensor functioning for monitoring of glucose in sweat. (**d**) Graph of current density changes in composite material under sweet consumption for glucose detection. Reprinted with permission from Ref. [186]. (**e**) SWASV response of composite material–based fabricated electrode for 300 ppb Cu (II) ion on normal and bending mode. (**f**) Photographs of bending processes of the fabricated electrode. Reproduced with permission from Ref. [187]. Copyright 2020, American Chemical Society.

4.2. Cortisol Sensing

Park et al. developed a microfluidic integrated wearable impedimetric immune sensor based on $Ti_3C_2T_x$ MXene incorporating laser-mediated porous graphene. This immune-sensing patch analyzes cortisol from the sweat by collecting sweat samples at one touch using a microfluidic channel network. Thus, wearable immune-sensing patches exhibit a dynamic range of 0.01–100 nM with a LOD of 88pM [188]. In another work, Laochai et al. fabricated Ti_3C_2 MXene/AuNPs/L-cysteine composited electrodes for real-time detection of cortisol from sweat [71]. Under optimal conditions, this fabricated sensor shows sensitivity with wide linearity of 5–180 ng mL^{-1} and a LOD value of 0.54 ng mL^{-1}. The real-time analysis of cortisol from artificial sweat results in a 94.47–102% recovery value. The fabrication of cortisol immune sensors and immobilization steps are discussed with the help of Figure 8a,b.

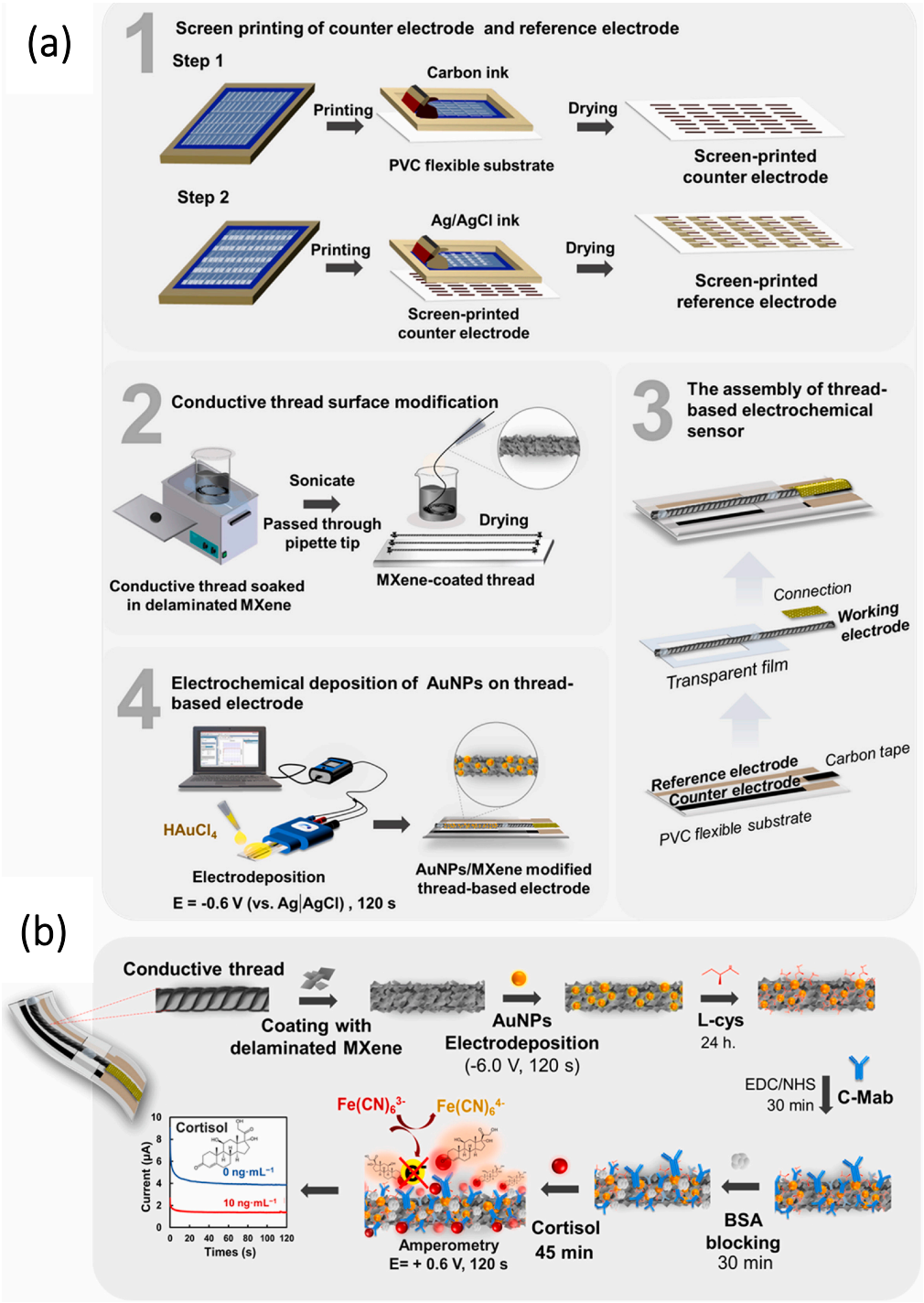


Figure 8. (**a**) Schematic illustration of the fabrication of counter and reference electrodes, surface modification, and electrochemical deposition of gold nanoparticles on the surface of the electrode. (**b**) Immobilization process. Reproduced with permission from Ref. [71]. Copyright 2022 Elsevier.

4.3. Other Analytes

Zhi et al. developed a bioinspired directional moisture-wicking electronic skin for static health monitoring with the support of triboelectric energy harvesting. The device is made of heterogeneous fibrous polyvinylidene fluoride (PVDF) as a hydrophobic layer and polyacrylonitrile (PAN) as the hydrophilic layer with $Ti_3C_2T_x$ MXene/CNT conductive ink [189]. Zhang et al. fabricated a wireless, battery-free, wearable, skin-interfaced electrochemical sensing patch for K^+ monitoring from sweat. They used valinomycin as a

K^+ selective carrier specific to K^+, enabling the selective detection of K^+ by the membrane. Figure 9a–e demonstrates the conceptual operation mechanism of the fabricated device, electrode fabrication, sensor fabrication, and CV analysis of the material, followed by EIS analysis. This fabricated sensor measures the K^+ ion concentration from human sweat with an excellent sensitivity of 63 mV/dec and a high linear detection range from 1 to 32 mM [77]. In another work, Hui et al. designed a flexible electrochemical heavy metal sensor for the non-invasive detection of Cu and Zn ions in human sweat with a material composition of $Ti_3C_2T_x$/multi-walled carbon nanotubes (MWCNTs) in a layer-by-layer self-assembly [187]. The square wave anodic stripping voltammetric method (SWASV) was used for electrochemical analysis. The resulting LOD of Cu and Zn ions is 0.1 and 1.5 ppb. The response of SWASV for Cu (II) ion and the bending process of the fabricated electrode are shown in Figure 7e,f.

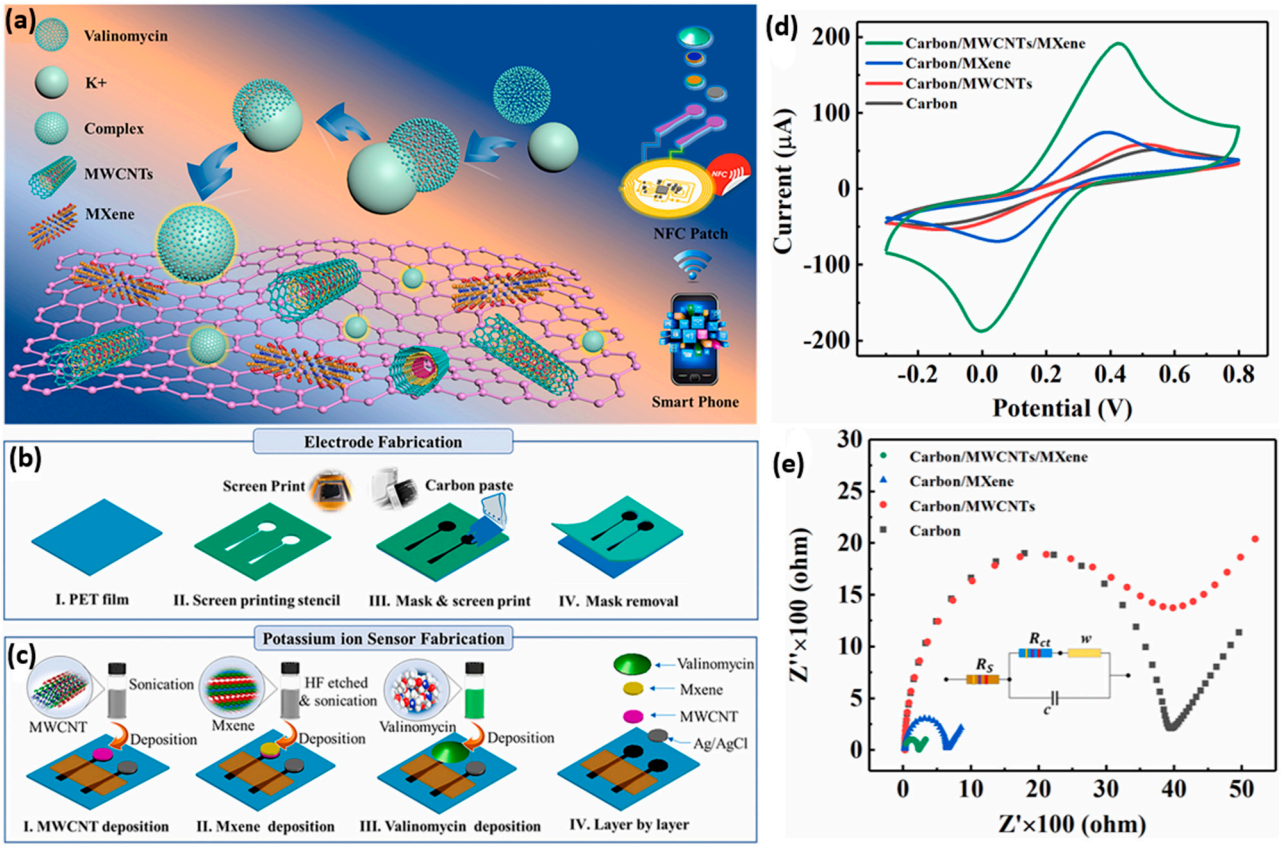


Figure 9. (**a**) Schematic illustration of the operating mechanism of wearable, wireless, battery–free integrated electrochemical sensing patch (valinomycin is a selective K^+ carrier and naturally has specific permeability to K^+). (**b**) Steps involved in electrode fabrication. (**c**) Sensor fabrication process. (**d**) CV study bare carbon, carbon/MWCNTs, carbon/MXene, and carbon/MWCNTs/MXene. (**e**) EIS Nyquist analysis. Reproduced with the permission form. Ref. [77]. Copyright 2020 Elsevier.

Cui et al. demonstrated a heterostructure Ti_3C_2 MXene/MoS_2 composite for detecting ascorbic acid in human sweat. The study resulted in high sensitivity of 54.6 nA μM^{-1} and a LOD of 4.2 μM [190]. In another work, Saleh et al. fabricated inkjet-printed $Ti_3C_2T_x$ MXene-based electrodes for cutaneous biosensing [74]. They demonstrated an exciting finding on Inkjet-printed MXene electrodes for Na^+ ion detection and cytokine protein with 3.9 mV per decade by simple changes in the functionalization of the target analyte. These findings simplify the fabrication of wearable electronic platforms that enable multimodal biosensing. Qiao et al. developed a Ti_3C_2 MXene@TiO_2 (anatase/rutile) ternary heterostructured electrode to detect phosphoprotein in sweat. They showed a LOD of 1.52 μM with a broad linear range from 0.01 to 1 mg/mL [191]. Chen et al. developed a flu-

oroalkyl functionalized F–$Ti_3C_2T_x$/polyaniline (PANI) superhydrophobic skin-attachable and wearable electrochemical pH biosensor for real-time perspiration analysis [192]. Thus, the schematic view of the sensing device setup, pH analysis of sweat in males/females, and comparison of measured values from the fabricated patch with other equipment are discussed in detail in Figure 10a–d.

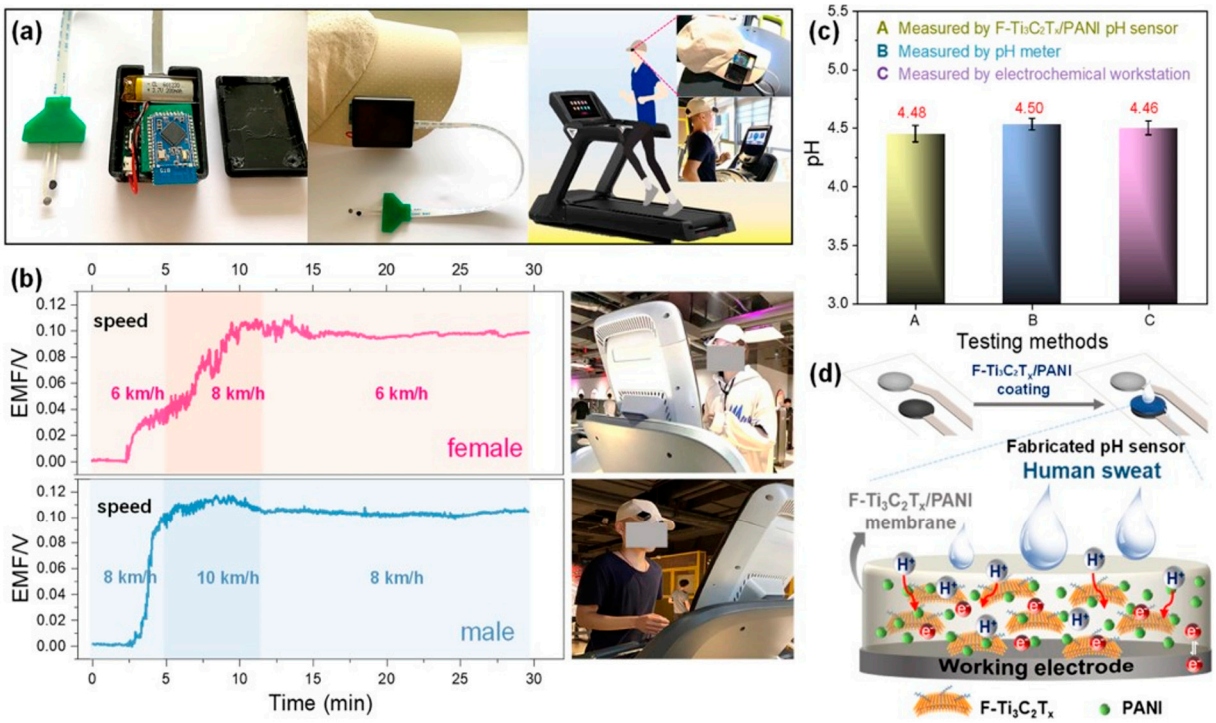


Figure 10. (**a**) Digital photograph of wearable pH sensor with a lithium-ion battery, mini–type potentiometer, and F–$Ti_3C_2T_x$/PANI material. (**b**) Continuously monitored real–time pH in human male and female volunteers. (**c**) Comparison of F–$Ti_3C_2T_x$/PANI sensor with ex situ electrochemical workstation and pH meter results. (**d**) Schematic illustration of F–$Ti_3C_2T_x$/PANI electrochemical behavior. Reproduced with permission from Ref. [192]. Copyright 2022 American Chemical Society.

5. Summary and Outlook

In recent years, more attention has been paid to MXenes due to their outstanding characteristic features such as high conductivity, surface area, oxidation and redox capacity, biocompatibility, and significant electrocatalytic and electrochemical properties. Moreover, MXenes also hold great potential as conductive substrates for various electrode-based devices, especially for specific-patterned electrodes. This paves the way for the fabrication of highly integrated electrochemical sensing gadgets such as wearable sensors for non-invasive monitoring of biomarkers in the body fluid (sweat) and miniaturized electronic devices for practical standards. However, for the faster translation of MXene-based electrochemical sensors from lab to market, we propose the following research directions in the near future:

(i) Device fabrication with precise nano-/micro-patterned structures are essential to enhance the performance of wearable sensors, and their shortcomings cannot be ignored [193].

(ii) It is challenging to synthesize MXenes on a large scale due to their atomic-thick layer design. To overcome this, future research should address the industrial-scale nanostructured design of MXenes and cost-effective technologies [194,195].

(iii) The malleable structure is crucial in changing the conductivity and internal resistance of the MXene. Hence future research should focus on the enlargement of interlayer distance in MXenes.

(iv) The problems with the flexibility of MXenes can be solved by performing focused research on MXene-polymer nanocomposites using biocompatible polymers [196].

(v) MXene-based biosensors strongly rely on nanohybrid biocompatibility. Thus, there should be focused research on the surface chemistry of MXenes to solve the problems based on the affinity and stability of biomolecules on MXene surfaces [197].

(vi) In the case of wearable sensors, MXene nanomaterial is oxidized when continuously in contact with air. This reduces the conductivity and affects the sensing ability. However, the external polymer coating to prevent oxidation in the MXene affects the breathability and comfort of the wearable biosensors. Thus, an in-depth understanding is needed to design sensors that could maintain the conductivity of the MXene without losing the convenience of the user [169].

Author Contributions: S.G. and A.P. conceptualized the paper; S.G. and K.R. wrote the paper; T.K. and A.P. reviewed and edited the manuscript. All authors have read and agreed to the published version of the manuscript.

Funding: The author (T.K) gratefully acknowledge the financial support of this project by the Ministry of Science and Technology, Taiwan (MOST 111-2221-E-027-085). A.P. would like to acknowledge the financial support from the Science and Engineering Research Board (SERB), Department of Science and Technology, Government of India for its start-up research grant (File No. SRG/2020/001115) scheme and expresses his appreciation to "VIT SEED GRANT". K.R. thank DST-INSPIRE JRF and SRF (Inspire Fellow No. IF210172) schemes for her Ph.D. fellowship.

Institutional Review Board Statement: Not applicable.

Informed Consent Statement: Not applicable.

Data Availability Statement: All the data and materials that support the results or analyses presented in their paper are freely available upon request.

Acknowledgments: The authors gratefully acknowledge the financial support of this project by the Ministry of Science and Technology, Taiwan (MOST 111-2221-E-027-085). S.G, A.P and K.R. would also like to acknowledge the support received from the Center for Biomaterials, Cellular, and Molecular Theranostics (CBCMT); the School of Advanced Sciences (SAS); and the Periyar Central Library of Vellore Institute of Technology, Vellore.

Conflicts of Interest: The authors declare no conflict of interest.

Sample Availability: Not applicable.

Abbreviations

cm	Centimeter
CNT	Carbon nanotube
CV	Cyclic voltammetry
CVD	Chemical vapor deposition
dec	Decade
DMSO	Dimethyl sulfoxide
DPV	Differential pulse voltammetry
ECG	Electrocardiogram
EIS	Electrochemical impendence spectroscopy
GCE	Glassy carbon electrode
HF	Hydrofluoric acid
KHF_2	Potassium bifluoride
LOD	Limit of detection
mL	Milliliter
mM	Millimolar
µM	Micromolar
MoS_2	Molybdenum disulfide
mV	Millivolts
MWCNT	Multi-walled carbon nanotube

$NaHF_2$	Sodium bifluoride
ng	Nanogram
NH_4^+	Ammonium
NH_4HF_2	Ammonium bifluoride
nM	Nanomolar
PAN	Polyacrylonitrile
PANI	Polyaniline
PET	Polyethylene terephthalate
PLD	Pulse laser deposition
pM	Picomolar
ppb	Parts per billion
PVDF	Polyvinylidene difluoride
SWASV	Square wave anodic stripping voltammetric method
TBAOH	Tetrabutylammonium hydroxide
TPAOH	Tetrapropylammonium hydroxide

References

1. Kim, J.; Campbell, A.S.; de Ávila, B.E.-F.; Wang, J. Wearable biosensors for healthcare monitoring. *Nat. Biotechnol.* **2019**, *37*, 389–406. [CrossRef] [PubMed]
2. Smith, A.A.; Li, R.; Tse, Z.T.H. Reshaping healthcare with wearable biosensors. *Sci. Rep.* **2023**, *13*, 4998. [CrossRef]
3. Grattieri, M.; Minteer, S.D. Self-Powered Biosensors. *ACS Sens.* **2018**, *3*, 44–53. [CrossRef]
4. Xiang, L.; Wang, Y.; Xia, F.; Liu, F.; He, D.; Long, G.; Zeng, X.; Liang, X.; Jin, C.; Wang, Y.; et al. An epidermal electronic system for physiological information acquisition, processing, and storage with an integrated flash memory array. *Sci. Adv.* **2023**, *8*, eabp8075. [CrossRef] [PubMed]
5. Kim, D.-H.; Lu, N.; Ma, R.; Kim, Y.-S.; Kim, R.-H.; Wang, S.; Wu, J.; Won, S.M.; Tao, H.; Islam, A.; et al. Epidermal Electronics. *Science* **2011**, *333*, 838–843. [CrossRef] [PubMed]
6. Ghaffari, R.; Choi, J.; Raj, M.S.; Chen, S.; Lee, S.P.; Reeder, J.T.; Aranyosi, A.J.; Leech, A.; Li, W.; Schon, S.; et al. Soft Wearable Systems for Colorimetric and Electrochemical Analysis of Biofluids. *Adv. Funct. Mater.* **2020**, *30*, 1907269. [CrossRef]
7. Singh, S.U.; Chatterjee, S.; Lone, S.A.; Ho, H.-H.; Kaswan, K.; Peringeth, K.; Khan, A.; Chiang, Y.-W.; Lee, S.; Lin, Z.-H. Advanced wearable biosensors for the detection of body fluids and exhaled breath by graphene. *Microchim. Acta* **2022**, *189*, 236. [CrossRef]
8. Wang, L.; Wang, J.; Fan, C.; Xu, T.; Zhang, X. Skin-like hydrogel-elastomer based electrochemical device for comfortable wearable biofluid monitoring. *Chem. Eng. J.* **2023**, *455*, 140609. [CrossRef]
9. Hong, Y.J.; Lee, H.; Kim, J.; Lee, M.; Choi, H.J.; Hyeon, T.; Kim, D.-H. Multifunctional Wearable System that Integrates Sweat-Based Sensing and Vital-Sign Monitoring to Estimate Pre-/Post-Exercise Glucose Levels. *Adv. Funct. Mater.* **2018**, *28*, 1805754. [CrossRef]
10. Wang, M.; Yang, Y.; Min, J.; Song, Y.; Tu, J.; Mukasa, D.; Ye, C.; Xu, C.; Heflin, N.; McCune, J.S.; et al. A wearable electrochemical biosensor for the monitoring of metabolites and nutrients. *Nat. Biomed. Eng.* **2022**, *6*, 1225–1235. [CrossRef]
11. Gómez, J.; Oviedo, B.; Zhuma, E. Patient Monitoring System Based on Internet of Things. *Procedia Comput. Sci.* **2016**, *83*, 90–97. [CrossRef]
12. Mohammadzadeh, N.; Safdari, R. Patient monitoring in mobile health: Opportunities and challenges. *Med. Arh.* **2014**, *68*, 57–60. [CrossRef]
13. Cameron, J.M.; Butler, H.J.; Palmer, D.S.; Baker, M.J. Biofluid spectroscopic disease diagnostics: A review on the processes and spectral impact of drying. *J. Biophotonics* **2018**, *11*, e201700299. [CrossRef] [PubMed]
14. Leal, L.B.; Nogueira, M.S.; Canevari, R.A.; Carvalho, L.F.C.S. Vibration spectroscopy and body biofluids: Literature review for clinical applications. *Photodiagn. Photodyn. Ther.* **2018**, *24*, 237–244. [CrossRef]
15. Shende, P.; Trivedi, R. Biofluidic material-based carriers: Potential systems for crossing cellular barriers. *J. Control. Release* **2021**, *329*, 858–870. [CrossRef] [PubMed]
16. Pucchio, A.; Krance, S.H.; Pur, D.R.; Miranda, R.N.; Felfeli, T. Artificial Intelligence Analysis of Biofluid Markers in Age-Related Macular Degeneration: A Systematic Review. *Clin. Ophthalmol.* **2022**, *16*, 2463–2476. [CrossRef]
17. Zafar, H.; Channa, A.; Jeoti, V.; Stojanović, G.M. Comprehensive Review on Wearable Sweat-Glucose Sensors for Continuous Glucose Monitoring. *Sensors* **2022**, *22*, 638. [CrossRef]
18. Derbyshire, P.J.; Barr, H.; Davis, F.; Higson, S.P.J. Lactate in human sweat: A critical review of research to the present day. *J. Physiol. Sci.* **2012**, *62*, 429–440. [CrossRef] [PubMed]
19. Huang, C.T.; Chen, M.L.; Huang, L.L.; Mao, I.F. Uric acid and urea in human sweat. *Chin. J. Physiol.* **2002**, *45*, 109–115.
20. Jones, A.P.; Webb, L.M.C.; Anderson, A.O.; Leonardo, E.J.; Rot, A. Normal human sweat contains interleukin-8. *J. Leukoc. Biol.* **1995**, *57*, 434–437. [CrossRef]
21. Itoh, S.; Nakayama, T. Ammonia in human sweat and its origin. *Jpn. J. Physiol.* **1952**, *3*, 133–137. [CrossRef]
22. Bates, G.P.; Miller, V.S. Sweat rate and sodium loss during work in the heat. *J. Occup. Med. Toxicol.* **2008**, *3*, 4. [CrossRef]

23. Vairo, D.; Bruzzese, L.; Marlinge, M.; Fuster, L.; Adjriou, N.; Kipson, N.; Brunet, P.; Cautela, J.; Jammes, Y.; Mottola, G.; et al. Towards Addressing the Body Electrolyte Environment via Sweat Analysis:Pilocarpine Iontophoresis Supports Assessment of Plasma Potassium Concentration. *Sci. Rep.* **2017**, *7*, 11801. [CrossRef] [PubMed]
24. Consolazio, C.F.; Matoush, L.O.; Nelson, R.A.; Hackler, L.R.; Preston, E.E. Relationship Between Calcium in Sweat, Calcium Balance, and Calcium Requirements. *J. Nutr.* **1962**, *78*, 78–88. [CrossRef]
25. Aruoma, O.I.; Reilly, T.; MacLaren, D.; Halliwell, B. Iron, copper and zinc concentrations in human sweat and plasma; the effect of exercise. *Clin. Chim. Acta* **1988**, *177*, 81–87. [CrossRef]
26. Stauber, J.L.; Florence, T.M. A comparative study of copper, lead, cadmium and zinc in human sweat and blood. *Sci. Total Environ.* **1988**, *74*, 235–247. [CrossRef]
27. Jia, W.; Bandodkar, A.J.; Valdés-Ramírez, G.; Windmiller, J.R.; Yang, Z.; Ramírez, J.; Chan, G.; Wang, J. Electrochemical tattoo biosensors for real-time noninvasive lactate monitoring in human perspiration. *Anal. Chem.* **2013**, *85*, 6553–6560. [CrossRef] [PubMed]
28. Bandodkar, A.J.; Wang, J. Non-invasive wearable electrochemical sensors: A review. *Trends Biotechnol.* **2014**, *32*, 363–371. [CrossRef] [PubMed]
29. Tabasum, H.; Gill, N.; Mishra, R.; Lone, S. Wearable microfluidic-based e-skin sweat sensors. *RSC Adv.* **2022**, *12*, 8691–8707. [CrossRef]
30. Mohan, A.M.V.; Rajendran, V.; Mishra, R.K.; Jayaraman, M. Recent advances and perspectives in sweat based wearable electrochemical sensors. *Trends Anal. Chem.* **2020**, *131*, 116024. [CrossRef]
31. Gao, F.; Liu, C.; Zhang, L.; Liu, T.; Wang, Z.; Song, Z.; Cai, H.; Fang, Z.; Chen, J.; Wang, J.; et al. Wearable and flexible electrochemical sensors for sweat analysis: A review. *Microsyst. Nanoeng.* **2023**, *9*, 1. [CrossRef] [PubMed]
32. Yang, P.; Wei, G.; Liu, A.; Huo, F.; Zhang, Z. A review of sampling, energy supply and intelligent monitoring for long-term sweat sensors. *NPJ Flex. Electron.* **2022**, *6*, 33. [CrossRef]
33. Kwon, K.; Kim, J.U.; Deng, Y.; Krishnan, S.R.; Choi, J.; Jang, H.; Lee, K.; Su, C.-J.; Yoo, I.; Wu, Y.; et al. An on-skin platform for wireless monitoring of flow rate, cumulative loss and temperature of sweat in real time. *Nat. Electron.* **2021**, *4*, 302–312. [CrossRef]
34. Krishnan, S.K.; Singh, E.; Singh, P.; Meyyappan, M.; Nalwa, H.S. A review on graphene-based nanocomposites for electrochemical and fluorescent biosensors. *RSC Adv.* **2019**, *9*, 8778–8881. [CrossRef] [PubMed]
35. Shao, Y.; Wang, J.; Wu, H.; Liu, J.; Aksay, I.A.; Lin, Y. Graphene Based Electrochemical Sensors and Biosensors: A Review. *Electroanalysis* **2010**, *22*, 1027–1036. [CrossRef]
36. Kokulnathan, T.; Wang, T.-J.; Kumar, E.A.; Duraisamy, N. An-Ting Lee An electrochemical platform based on yttrium oxide/boron nitride nanocomposite for the detection of dopamine. *Sens. Actuators B Chem.* **2021**, *349*, 130787. [CrossRef]
37. Kokulnathan, T.; Ahmed, F.; Chen, S.-M.; Chen, T.-W.; Hasan, P.M.Z.; Bilgrami, A.L.; Darwesh, R. Rational Confinement of Yttrium Vanadate within Three-Dimensional Graphene Aerogel: Electrochemical Analysis of Monoamine Neurotransmitter (Dopamine). *ACS Appl. Mater. Interfaces* **2021**, *13*, 10987–10995. [CrossRef]
38. Agnihotri, A.S.; Varghese, A.; Nidhin, M. Transition metal oxides in electrochemical and bio sensing: A state-of-art review. *Appl. Surf. Sci. Adv.* **2021**, *4*, 100072. [CrossRef]
39. Xu, M.; Song, Y.; Wang, J.; Li, N. Anisotropic transition metal–based nanomaterials for biomedical applications. *VIEW* **2021**, *2*, 20200154. [CrossRef]
40. Wang, Y.-H.; Huang, K.-J.; Wu, X. Recent advances in transition-metal dichalcogenides based electrochemical biosensors: A review. *Biosens. Bioelectron.* **2017**, *97*, 305–316. [CrossRef]
41. Mia, A.K.; Meyyappan, M.; Giri, P.K. Two-Dimensional Transition Metal Dichalcogenide Based Biosensors: From Fundamentals to Healthcare Applications. *Biosensors* **2023**, *13*, 169. [CrossRef]
42. Hegde, M.; Pai, P.; Shetty, M.G.; Babitha, K.S. Gold nanoparticle based biosensors for rapid pathogen detection: A review. *Environ. Nanotechnol. Monit. Manag.* **2022**, *18*, 100756. [CrossRef]
43. Nooranian, S.; Mohammadinejad, A.; Mohajeri, T.; Aleyaghoob, G.; Kazemi Oskuee, R. Biosensors based on aptamer-conjugated gold nanoparticles: A review. *Biotechnol. Appl. Biochem.* **2022**, *69*, 1517–1534. [CrossRef]
44. Beck, F.; Loessl, M.; Baeumner, A.J. Signaling strategies of silver nanoparticles in optical and electrochemical biosensors: Considering their potential for the point-of-care. *Microchim. Acta* **2023**, *190*, 91. [CrossRef] [PubMed]
45. Tan, P.; Li, H.; Wang, J.; Gopinath, S.C.B. Silver nanoparticle in biosensor and bioimaging: Clinical perspectives. *Biotechnol. Appl. Biochem.* **2021**, *68*, 1236–1242. [CrossRef]
46. Amara, U.; Hussain, I.; Ahmad, M.; Mahmood, K.; Zhang, K. 2D MXene-Based Biosensing: A Review. *Small* **2023**, *19*, 2205249. [CrossRef]
47. Gogotsi, Y.; Anasori, B. The Rise of MXenes. *ACS Nano* **2019**, *13*, 8491–8494. [CrossRef] [PubMed]
48. Ankitha, M.; Arjun, A.M.; Shabana, N.; Rasheed, P.A. A Mini Review on Recent Advances in MXene Based Electrochemical Wearable Sensing Devices. *Biomed. Mater. Devices* **2022**. [CrossRef]
49. Wang, Q.; Han, N.; Shen, Z.; Li, X.; Chen, Z.; Cao, Y.; Si, W.; Wang, F.; Ni, B.-J.; Thakur, V.K. MXene-based electrochemical (bio) sensors for sustainable applications: Roadmap for future advanced materials. *Nano Mater. Sci.* **2023**, *5*, 39–52. [CrossRef]
50. Alnoor, H.; Elsukova, A.; Palisaitis, J.; Persson, I.; Tseng, E.N.; Lu, J.; Hultman, L.; Persson, P.O.Å. Exploring MXenes and their MAX phase precursors by electron microscopy. *Mater. Today Adv.* **2021**, *9*, 100123. [CrossRef]

51. Buono, M.J. Sweat Ethanol Concentrations are Highly Correlated with Co-Existing Blood Values in Humans. *Exp. Physiol.* **1999**, *84*, 401–404. [CrossRef]
52. Fogh-Andersen, N.; Altura, B.M.; Altura, B.T.; Siggaard-Andersen, O. Composition of interstitial fluid. *Clin. Chem.* **1995**, *41*, 1522–1525. [CrossRef] [PubMed]
53. Bariya, M.; Nyein, H.Y.Y.; Javey, A. Wearable sweat sensors. *Nat. Electron.* **2018**, *1*, 160–171. [CrossRef]
54. Mannoor, M.S.; Tao, H.; Clayton, J.D.; Sengupta, A.; Kaplan, D.L.; Naik, R.R.; Verma, N.; Omenetto, F.G.; McAlpine, M.C. Graphene-based wireless bacteria detection on tooth enamel. *Nat. Commun.* **2012**, *3*, 763. [CrossRef] [PubMed]
55. Ravishankar, P.; Daily, A. Tears as the Next Diagnostic Biofluid: A Comparative Study between Ocular Fluid and Blood. *Appl. Sci.* **2022**, *12*, 2884. [CrossRef]
56. Fishberg, E.H.; Bierman, W. Acid-Base Balance in Sweat. *J. Biol. Chem.* **1932**, *97*, 433–441. [CrossRef]
57. Shiohara, T.; Mizukawa, Y.; Shimoda-Komatsu, Y.; Aoyama, Y. Sweat is a most efficient natural moisturizer providing protective immunity at points of allergen entry. *Allergol. Int.* **2018**, *67*, 442–447. [CrossRef]
58. Bandodkar, A.J.; Jeerapan, I.; Wang, J. Wearable Chemical Sensors: Present Challenges and Future Prospects. *ACS Sens.* **2016**, *1*, 464–482. [CrossRef]
59. Choi, J.; Ghaffari, R.; Baker, L.B.; Rogers, J.A. Skin-interfaced systems for sweat collection and analytics. *Sci. Adv.* **2023**, *4*, eaar3921. [CrossRef]
60. Legner, C.; Kalwa, U.; Patel, V.; Chesmore, A.; Pandey, S. Sweat sensing in the smart wearables era: Towards integrative, multifunctional and body-compliant perspiration analysis. *Sens. Actuators A Phys.* **2019**, *296*, 200–221. [CrossRef]
61. Emaminejad, S.; Gao, W.; Wu, E.; Davies, Z.A.; Yin Yin Nyein, H.; Challa, S.; Ryan, S.P.; Fahad, H.M.; Chen, K.; Shahpar, Z.; et al. Autonomous sweat extraction and analysis applied to cystic fibrosis and glucose monitoring using a fully integrated wearable platform. *Proc. Natl. Acad. Sci. USA* **2017**, *114*, 4625–4630. [CrossRef] [PubMed]
62. Zhao, Y.; Zhai, Q.; Dong, D.; An, T.; Gong, S.; Shi, Q.; Cheng, W. Highly Stretchable and Strain-Insensitive Fiber-Based Wearable Electrochemical Biosensor to Monitor Glucose in the Sweat. *Anal. Chem.* **2019**, *91*, 6569–6576. [CrossRef] [PubMed]
63. Komkova, M.A.; Eliseev, A.A.; Poyarkov, A.A.; Daboss, E.V.; Evdokimov, P.V.; Eliseev, A.A.; Karyakin, A.A. Simultaneous monitoring of sweat lactate content and sweat secretion rate by wearable remote biosensors. *Biosens. Bioelectron.* **2022**, *202*, 113970. [CrossRef] [PubMed]
64. Gao, W.; Emaminejad, S.; Nyein, H.Y.Y.; Challa, S.; Chen, K.; Peck, A.; Fahad, H.M.; Ota, H.; Shiraki, H.; Kiriya, D.; et al. Fully integrated wearable sensor arrays for multiplexed in situ perspiration analysis. *Nature* **2016**, *529*, 509–514. [CrossRef]
65. Al-Tamer, Y.Y.; Hadi, E.A.; Al-Badrani, I. eldin I. Sweat urea, uric acid and creatinine concentrations in uraemic patients. *Urol. Res.* **1997**, *25*, 337–340. [CrossRef]
66. Gao, W.; Nyein, H.Y.Y.; Shahpar, Z.; Fahad, H.M.; Chen, K.; Emaminejad, S.; Gao, Y.; Tai, L.-C.; Ota, H.; Wu, E.; et al. Wearable Microsensor Array for Multiplexed Heavy Metal Monitoring of Body Fluids. *ACS Sens.* **2016**, *1*, 866–874. [CrossRef]
67. Kim, J.; de Araujo, W.R.; Samek, I.A.; Bandodkar, A.J.; Jia, W.; Brunetti, B.; Paixão, T.R.L.C.; Wang, J. Wearable temporary tattoo sensor for real-time trace metal monitoring in human sweat. *Electrochem. Commun.* **2015**, *51*, 41–45. [CrossRef]
68. Yang, Q.; Rosati, G.; Abarintos, V.; Aroca, M.A.; Osma, J.F.; Merkoçi, A. Wearable and fully printed microfluidic nanosensor for sweat rate, conductivity, and copper detection with healthcare applications. *Biosens. Bioelectron.* **2022**, *202*, 114005. [CrossRef]
69. Munje, R.D.; Muthukumar, S.; Jagannath, B.; Prasad, S. A new paradigm in sweat based wearable diagnostics biosensors using Room Temperature Ionic Liquids (RTILs). *Sci. Rep.* **2017**, *7*, 1950. [CrossRef]
70. Gaines Das, R.E.; Poole, S. The international standard for interleukin-6: Evaluation in an international collaborative study. *J. Immunol. Methods* **1993**, *160*, 147–153. [CrossRef]
71. Laochai, T.; Yukird, J.; Promphet, N.; Qin, J.; Chailapakul, O.; Rodthongkum, N. Non-invasive electrochemical immunosensor for sweat cortisol based on L-cys/AuNPs/ MXene modified thread electrode. *Biosens. Bioelectron.* **2022**, *203*, 114039. [CrossRef] [PubMed]
72. Cizza, G.; Marques, A.H.; Eskandari, F.; Christie, I.C.; Torvik, S.; Silverman, M.N.; Phillips, T.M.; Sternberg, E.M. Elevated Neuroimmune Biomarkers in Sweat Patches and Plasma of Premenopausal Women with Major Depressive Disorder in Remission: The POWER Study. *Biol. Psychiatry* **2008**, *64*, 907–911. [CrossRef] [PubMed]
73. Zahed, M.A.; Sharifuzzaman, M.; Yoon, H.; Asaduzzaman, M.; Kim, D.K.; Jeong, S.; Pradhan, G.B.; Shin, Y.D.; Yoon, S.H.; Sharma, S.; et al. A Nanoporous Carbon-MXene Heterostructured Nanocomposite-Based Epidermal Patch for Real-Time Biopotentials and Sweat Glucose Monitoring. *Adv. Funct. Mater.* **2022**, *32*, 2208344. [CrossRef]
74. Saleh, A.; Wustoni, S.; Bihar, E.; El-demellawi, J.K.; Zhang, Y.; Hama, A. Inkjet-printed $Ti_3C_2T_x$ MXene electrodes for multimodal cutaneous biosensing. *J. Phys.* **2020**, *3*, 044004. [CrossRef]
75. Dang, W.; Manjakkal, L.; Navaraj, W.T.; Lorenzelli, L.; Vinciguerra, V.; Dahiya, R. Stretchable wireless system for sweat pH monitoring. *Biosens. Bioelectron.* **2018**, *107*, 192–202. [CrossRef] [PubMed]
76. Rosenstein, B.J.; Cutting, G.R. The diagnosis of cystic fibrosis: A consensus statement. Cystic Fibrosis Foundation Consensus Panel. *J. Pediatr.* **1998**, *132*, 589–595. [CrossRef]
77. Zhang, S.; Zahed, M.A.; Sharifuzzaman, M.; Yoon, S.; Hui, X.; Chandra Barman, S.; Sharma, S.; Yoon, H.S.; Park, C.; Park, J.Y. A wearable battery-free wireless and skin-interfaced microfluidics integrated electrochemical sensing patch for on-site biomarkers monitoring in human perspiration. *Biosens. Bioelectron.* **2021**, *175*, 112844. [CrossRef]

78. Nyein, H.Y.Y.; Gao, W.; Shahpar, Z.; Emaminejad, S.; Challa, S.; Chen, K.; Fahad, H.M.; Tai, L.-C.; Ota, H.; Davis, R.W.; et al. A Wearable Electrochemical Platform for Noninvasive Simultaneous Monitoring of Ca^{2+} and pH. *ACS Nano* **2016**, *10*, 7216–7224. [CrossRef]
79. Terse-Thakoor, T.; Punjiya, M.; Matharu, Z.; Lyu, B.; Ahmad, M.; Giles, G.E.; Owyeung, R.; Alaimo, F.; Shojaei Baghini, M.; Brunyé, T.T.; et al. Thread-based multiplexed sensor patch for real-time sweat monitoring. *NPJ Flex. Electron.* **2020**, *4*, 18. [CrossRef]
80. Guinovart, T.; Bandodkar, A.J.; Windmiller, J.R.; Andrade, F.J.; Wang, J. A potentiometric tattoo sensor for monitoring ammonium in sweat. *Analyst* **2013**, *138*, 7031–7038. [CrossRef]
81. Radecki, J.; Radecka, H. Voltammetric Biosensors in Bioanalysis BT. In *Handbook of Bioanalytics*; Buszewski, B., Baranowska, I., Eds.; Springer International Publishing: Cham, Switzerland, 2022; pp. 747–760. ISBN 978-3-030-95660-8.
82. Yunus, S.; Jonas, A.M.; Lakard, B. Potentiometric Biosensors BT. In *Encyclopedia of Biophysics*; Roberts, G.C.K., Ed.; Springer: Berlin/Heidelberg, Germany, 2013; pp. 1941–1946.
83. Sadeghi, S.J. Amperometric Biosensors BT. In *Encyclopedia of Biophysics*; Roberts, G.C.K., Ed.; Springer: Berlin/Heidelberg, Germany, 2013; pp. 61–67.
84. Radhakrishnan, R.; Suni, I.I.; Bever, C.S.; Hammock, B.D. Impedance Biosensors: Applications to Sustainability and Remaining Technical Challenges. *ACS Sustain. Chem. Eng.* **2014**, *2*, 1649–1655. [CrossRef] [PubMed]
85. Naguib, M.; Kurtoglu, M.; Presser, V.; Lu, J.; Niu, J.; Heon, M.; Hultman, L.; Gogotsi, Y.; Barsoum, M.W. Two-Dimensional Nanocrystals Produced by Exfoliation of Ti_3AlC_2. *Adv. Mater.* **2011**, *23*, 4248–4253. [CrossRef] [PubMed]
86. Meshkian, R.; Näslund, L.-Å.; Halim, J.; Lu, J.; Barsoum, M.W.; Rosen, J. Synthesis of two-dimensional molybdenum carbide, Mo_2C, from the gallium based atomic laminate Mo_2Ga_2C. *Scr. Mater.* **2015**, *108*, 147–150. [CrossRef]
87. Hu, T.; Hu, M.; Li, Z.; Zhang, H.; Zhang, C.; Wang, J.; Wang, X. Interlayer coupling in two-dimensional titanium carbide MXenes. *Phys. Chem. Chem. Phys.* **2016**, *18*, 20256–20260. [CrossRef]
88. Malaki, M.; Maleki, A.; Varma, R.S. MXenes and ultrasonication. *J. Mater. Chem. A* **2019**, *7*, 10843–10857. [CrossRef]
89. Zhang, W.; Zhang, X. The effect of ultrasound on synthesis and energy storage mechanism of $Ti_3C_2T_x$ MXene. *Ultrason. Sonochem.* **2022**, *89*, 106122. [CrossRef]
90. Lipatov, A.; Alhabeb, M.; Lukatskaya, M.R.; Boson, A.; Gogotsi, Y.; Sinitskii, A. Effect of Synthesis on Quality, Electronic Properties and Environmental Stability of Individual Monolayer Ti_3C_2 MXene Flakes. *Adv. Electron. Mater.* **2016**, *2*, 1600255. [CrossRef]
91. Zhang, T.; Chang, L.; Zhang, X.; Wan, H.; Liu, N.; Zhou, L.; Xiao, X. Simultaneously tuning interlayer spacing and termination of MXenes by Lewis-basic halides. *Nat. Commun.* **2022**, *13*, 6731. [CrossRef]
92. Li, C.; Xue, Z.; Qin, J.; Sawangphruk, M.; Yu, P.; Zhang, X.; Liu, R. Synthesis of nickel hydroxide/delaminated-Ti_3C_2 MXene nanosheets as promising anode material for high performance lithium ion battery. *J. Alloys Compd.* **2020**, *842*, 155812. [CrossRef]
93. Lv, G.; Wang, J.; Shi, Z.; Fan, L. Intercalation and delamination of two-dimensional MXene ($Ti_3C_2T_x$) and application in sodium-ion batteries. *Mater. Lett.* **2018**, *219*, 45–50. [CrossRef]
94. Liu, L.; Orbay, M.; Luo, S.; Duluard, S.; Shao, H.; Harmel, J.; Rozier, P.; Taberna, P.-L.; Simon, P. Exfoliation and Delamination of $Ti_3C_2T_x$ MXene Prepared via Molten Salt Etching Route. *ACS Nano* **2022**, *16*, 111–118. [CrossRef]
95. Lin, H.; Gao, S.; Dai, C.; Chen, Y.; Shi, J. A Two-Dimensional Biodegradable Niobium Carbide (MXene) for Photothermal Tumor Eradication in NIR-I and NIR-II Biowindows. *J. Am. Chem. Soc.* **2017**, *139*, 16235–16247. [CrossRef]
96. Li, G.; Tan, L.; Zhang, Y.; Wu, B.; Li, L. Highly Efficiently Delaminated Single-Layered MXene Nanosheets with Large Lateral Size. *Langmuir* **2017**, *33*, 9000–9006. [CrossRef]
97. Chen, X.; Zhu, Y.; Zhang, M.; Sui, J.; Peng, W.; Li, Y.; Zhang, G.; Zhang, F.; Fan, X. N-Butyllithium-Treated $Ti_3C_2T_x$ MXene with Excellent Pseudocapacitor Performance. *ACS Nano* **2019**, *13*, 9449–9456. [CrossRef] [PubMed]
98. Seredych, M.; Maleski, K.; Mathis, T.S.; Gogotsi, Y. Delamination of MXenes using bovine serum albumin. *Colloids Surfaces A Physicochem. Eng. Asp.* **2022**, *641*, 128580. [CrossRef]
99. Kumar, S.; Kang, D.; Hong, H.; Rehman, M.A.; Lee, Y.; Lee, N.; Seo, Y. Effect of $Ti_3C_2T_x$ MXenes etched at elevated temperatures using concentrated acid on binder-free supercapacitors. *RSC Adv.* **2020**, *10*, 41837–41845. [CrossRef]
100. Omulepu, O.; Bryan, D.J. Chapter 100—Chemical Injuries. In *Plastic Surgery Secrets Plus*, 2nd ed.; Weinzweig, J., Ed.; Mosby: Philadelphia, MS, USA, 2010; pp. 652–656. ISBN 978-0-323-03470-8.
101. Gad, S.E.; Sullivan, D.W. Hydrofluoric Acid. In *Encyclopedia of Toxicology*, 3rd ed.; Wexler, P., Ed.; Academic Press: Oxford, UK, 2014; pp. 964–966. ISBN 978-0-12-386455-0.
102. Dai, H.; Shi, S.; Yang, L.; Guo, C.; Chen, X. Recent progress on the corrosion behavior of metallic materials in HF solution. *Corros. Rev.* **2021**, *39*, 313–337. [CrossRef]
103. Feng, A.; Yu, Y.; Wang, Y.; Jiang, F.; Yu, Y.; Mi, L.; Song, L. Two-dimensional MXene Ti_3C_2 produced by exfoliation of Ti_3AlC_2. *Mater. Des.* **2017**, *114*, 161–166. [CrossRef]
104. Venkateshalu, S.; Grace, A.N. MXenes—A new class of 2D layered materials: Synthesis, properties, applications as supercapacitor electrode and beyond. *Appl. Mater. Today* **2020**, *18*, 100509. [CrossRef]
105. Li, H.; Fan, R.; Zou, B.; Yan, J.; Shi, Q.; Guo, G. Roles of MXenes in biomedical applications: Recent developments and prospects. *J. Nanobiotechnol.* **2023**, *21*, 73. [CrossRef] [PubMed]
106. Urbankowski, P.; Anasori, B.; Makaryan, T.; Er, D.; Kota, S.; Walsh, P.L.; Zhao, M.; Shenoy, V.B.; Barsoum, M.W.; Gogotsi, Y. Synthesis of two-dimensional titanium nitride Ti_4N_3 (MXene). *Nanoscale* **2016**, *8*, 11385–11391. [CrossRef] [PubMed]

107. Björk, J.; Rosen, J. Functionalizing MXenes by Tailoring Surface Terminations in Different Chemical Environments. *Chem. Mater.* **2021**, *33*, 9108–9118. [CrossRef]
108. Huang, K.; Li, Z.; Lin, J.; Han, G.; Huang, P. Two-dimensional transition metal carbides and nitrides (MXenes) for biomedical applications. *Chem. Soc. Rev.* **2018**, *47*, 5109–5124. [CrossRef]
109. Verger, L.; Xu, C.; Natu, V.; Cheng, H.-M.; Ren, W.; Barsoum, M.W. Overview of the synthesis of MXenes and other ultrathin 2D transition metal carbides and nitrides. *Curr. Opin. Solid State Mater. Sci.* **2019**, *23*, 149–163. [CrossRef]
110. Shen, B.; Huang, H.; Liu, H.; Jiang, Q.; He, H. Bottom-up construction of three-dimensional porous MXene/nitrogen-doped graphene architectures as efficient hydrogen evolution electrocatalysts. *Int. J. Hydrogen Energy* **2021**, *46*, 29984–29993. [CrossRef]
111. Jiang, L.; Zhou, D.; Yang, J.; Zhou, S.; Wang, H.; Yuan, X.; Liang, J.; Li, X.; Chen, Y.; Li, H. 2D single- and few-layered MXenes: Synthesis, applications and perspectives. *J. Mater. Chem. A* **2022**, *10*, 13651–13672. [CrossRef]
112. Hong, Y.-L.; Liu, Z.; Wang, L.; Zhou, T.; Ma, W.; Xu, C.; Feng, S.; Chen, L.; Chen, M.-L.; Sun, D.-M.; et al. Chemical vapor deposition of layered two-dimensional $MoSi_2N_4$ materials. *Science* **2020**, *369*, 670–674. [CrossRef]
113. Xu, C.; Wang, L.; Liu, Z.; Chen, L.; Guo, J.; Kang, N.; Ma, X.-L.; Cheng, H.-M.; Ren, W. Large-area high-quality 2D ultrathin Mo_2C superconducting crystals. *Nat. Mater.* **2015**, *14*, 1135–1141. [CrossRef]
114. Turker, F.; Caylan, O.R.; Mehmood, N.; Kasirga, T.S.; Sevik, C.; Cambaz Buke, G. CVD synthesis and characterization of thin Mo_2C crystals. *J. Am. Ceram. Soc.* **2020**, *103*, 5586–5593. [CrossRef]
115. Zhang, Z.; Zhang, F.; Wang, H.; Chan, C.H.; Lu, W.; Dai, J. Substrate orientation-induced epitaxial growth of face centered cubic Mo_2C superconductive thin film. *J. Mater. Chem. C* **2017**, *5*, 10822–10827. [CrossRef]
116. Xiao, X.; Yu, H.; Jin, H.; Wu, M.; Fang, Y.; Sun, J.; Hu, Z.; Li, T.; Wu, J.; Huang, L.; et al. Salt-Templated Synthesis of 2D Metallic MoN and Other Nitrides. *ACS Nano* **2017**, *11*, 2180–2186. [CrossRef]
117. Bai, S.; Yang, M.; Jiang, J.; He, X.; Zou, J.; Xiong, Z.; Liao, G.; Liu, S. Recent advances of MXenes as electrocatalysts for hydrogen evolution reaction. *NPJ 2D Mater. Appl.* **2021**, *5*, 78. [CrossRef]
118. Wu, L.; Yuan, X.; Tang, Y.; Wageh, S.; Al-Hartomy, O.A.; Al-Sehemi, A.G.; Yang, J.; Xiang, Y.; Zhang, H.; Qin, Y. MXene sensors based on optical and electrical sensing signals: From biological, chemical, and physical sensing to emerging intelligent and bionic devices. *PhotoniX* **2023**, *4*, 15. [CrossRef]
119. Bhardwaj, S.K.; Singh, H.; Khatri, M.; Kim, K.-H.; Bhardwaj, N. Advances in MXenes-based optical biosensors: A review. *Biosens. Bioelectron.* **2022**, *202*, 113995. [CrossRef]
120. Wu, X.; Ma, P.; Sun, Y.; Du, F.; Song, D.; Xu, G. Application of MXene in Electrochemical Sensors: A Review. *Electroanalysis* **2021**, *33*, 1827–1851. [CrossRef]
121. Joseph, X.B.; Baby, J.N.; Wang, S.-F.; Sriram, B.; George, M. Interfacial Superassembly of Mo_2C@NiMn-LDH Frameworks for Electrochemical Monitoring of Carbendazim Fungicide. *ACS Sustain. Chem. Eng.* **2021**, *9*, 14900–14910. [CrossRef]
122. Kokulnathan, T.; Wang, T.-J. Vanadium Carbide-Entrapped Graphitic Carbon Nitride Nanocomposites: Synthesis and Electrochemical Platforms for Accurate Detection of Furazolidone. *ACS Appl. Nano Mater.* **2020**, *3*, 2554–2561. [CrossRef]
123. Kokulnathan, T.; Wang, T.-J.; Ahmed, F.; Kumar, S. Deep eutectic solvents-assisted synthesis of NiFe-LDH/Mo_2C nanocomposite for electrochemical determination of nitrite. *J. Mol. Liq.* **2023**, *369*, 120785. [CrossRef]
124. Kokulnathan, T.; Wang, T.-J.; Ahmed, F.; Alshahrani, T. Hydrothermal synthesis of ZnCr-LDH/Tungsten carbide composite: A disposable electrochemical strip for mesalazine analysis. *Chem. Eng. J.* **2023**, *451*, 138884. [CrossRef]
125. Kokulnathan, T.; Ashok Kumar, E.; Wang, T.-J. Design and In Situ Synthesis of Titanium Carbide/Boron Nitride Nanocomposite: Investigation of Electrocatalytic Activity for the Sulfadiazine Sensor. *ACS Sustain. Chem. Eng.* **2020**, *8*, 12471–12481. [CrossRef]
126. Kumar, E.A.; Kokulnathan, T.; Wang, T.-J.; Anthuvan, A.J.; Chang, Y.-H. Two-dimensional titanium carbide (MXene) nanosheets as an efficient electrocatalyst for 4-nitroquinoline N-oxide detection. *J. Mol. Liq.* **2020**, *312*, 113354. [CrossRef]
127. Yoo, S.S.; Ho, J.-W.; Shin, D.-I.; Kim, M.; Hong, S.; Lee, J.H.; Jeong, H.J.; Jeong, M.S.; Yi, G.-R.; Kwon, S.J.; et al. Simultaneously intensified plasmonic and charge transfer effects in surface enhanced Raman scattering sensors using an MXene-blanketed Au nanoparticle assembly. *J. Mater. Chem. A* **2022**, *10*, 2945–2956. [CrossRef]
128. Satheeshkumar, E.; Makaryan, T.; Melikyan, A.; Minassian, H.; Gogotsi, Y.; Yoshimura, M. One-step Solution Processing of Ag, Au and Pd@MXene Hybrids for SERS. *Sci. Rep.* **2016**, *6*, 32049. [CrossRef] [PubMed]
129. Huang, J.; Li, Z.; Mao, Y.; Li, Z. Progress and biomedical applications of MXenes. *Nano Sel.* **2021**, *2*, 1480–1508. [CrossRef]
130. Ganesan, S.; Ethiraj, K.R.; Kesarla, M.K.; Palaniappan, A. Biomedical Applications of MXenes BT. In *Fundamental Aspects and Perspectives of MXenes*; Khalid, M., Grace, A.N., Arulraj, A., Numan, A., Eds.; Springer International Publishing: Cham, Switzerland, 2022; pp. 271–300. ISBN 978-3-031-05006-0.
131. Song, P.; Liu, B.; Qiu, H.; Shi, X.; Cao, D.; Gu, J. MXenes for polymer matrix electromagnetic interference shielding composites: A review. *Compos. Commun.* **2021**, *24*, 100653. [CrossRef]
132. Liang, L.; Yao, C.; Yan, X.; Feng, Y.; Hao, X.; Zhou, B.; Wang, Y.; Ma, J.; Liu, C.; Shen, C. High-efficiency electromagnetic interference shielding capability of magnetic $Ti_3C_2T_x$ MXene/CNT composite film. *J. Mater. Chem. A* **2021**, *9*, 24560–24570. [CrossRef]
133. Han, M.; Shuck, C.E.; Rakhmanov, R.; Parchment, D.; Anasori, B.; Koo, C.M.; Friedman, G.; Gogotsi, Y. Beyond $Ti_3C_2T_x$: MXenes for Electromagnetic Interference Shielding. *ACS Nano* **2020**, *14*, 5008–5016. [CrossRef]
134. Liu, S.; Song, Z.; Jin, X.; Mao, R.; Zhang, T.; Hu, F. MXenes for metal-ion and metal-sulfur batteries: Synthesis, properties, and electrochemistry. *Mater. Rep. Energy* **2022**, *2*, 100077. [CrossRef]

135. Anasori, B.; Lukatskaya, M.R.; Gogotsi, Y. 2D metal carbides and nitrides (MXenes) for energy storage. *Nat. Rev. Mater.* **2017**, *2*, 16098. [CrossRef]
136. Firestein, K.L.; von Treifeldt, J.E.; Kvashnin, D.G.; Fernando, J.F.S.; Zhang, C.; Kvashnin, A.G.; Podryabinkin, E.V.; Shapeev, A.V.; Siriwardena, D.P.; Sorokin, P.B.; et al. Young's Modulus and Tensile Strength of Ti_3C_2 MXene Nanosheets as Revealed by In Situ TEM Probing, AFM Nanomechanical Mapping, and Theoretical Calculations. *Nano Lett.* **2020**, *20*, 5900–5908. [CrossRef]
137. Lipatov, A.; Lu, H.; Alhabeb, M.; Anasori, B.; Gruverman, A.; Gogotsi, Y.; Sinitskii, A. Elastic properties of 2D $Ti_3C_2T_x$ MXene monolayers and bilayers. *Sci. Adv.* **2018**, *4*, eaat0491. [CrossRef] [PubMed]
138. Zhang, Y.; Xia, W.; Wu, Y.; Zhang, P. Prediction of MXene based 2D tunable band gap semiconductors: GW quasiparticle calculations. *Nanoscale* **2019**, *11*, 3993–4000. [CrossRef] [PubMed]
139. Yu, L.; Huang, D.; Wang, X.; Yu, W.; Yue, Y. Tuning thermal and electrical properties of MXenes via dehydration. *Phys. Chem. Chem. Phys.* **2022**, *24*, 25969–25978. [CrossRef] [PubMed]
140. Peng, Y.; Cai, P.; Yang, L.; Liu, Y.; Zhu, L.; Zhang, Q.; Liu, J.; Huang, Z.; Yang, Y. Theoretical and Experimental Studies of Ti_3C_2 MXene for Surface-Enhanced Raman Spectroscopy-Based Sensing. *ACS Omega* **2020**, *5*, 26486–26496. [CrossRef]
141. Khazaei, M.; Ranjbar, A.; Arai, M.; Sasaki, T.; Yunoki, S. Electronic properties and applications of MXenes: A theoretical review. *J. Mater. Chem. C* **2017**, *5*, 2488–2503. [CrossRef]
142. Li, T.; Yan, X.; Huang, L.; Li, J.; Yao, L.; Zhu, Q.; Wang, W.; Abbas, W.; Naz, R.; Gu, J.; et al. Fluorine-free $Ti_3C_2T_x$ (T = O, OH) nanosheets (∼50–100 nm) for nitrogen fixation under ambient conditions. *J. Mater. Chem. A* **2019**, *7*, 14462–14465. [CrossRef]
143. Enyashin, A.N.; Ivanovskii, A.L. Atomic structure, comparative stability and electronic properties of hydroxylated Ti_2C and Ti_3C_2 nanotubes. *Comput. Theor. Chem.* **2012**, *989*, 27–32. [CrossRef]
144. Hart, J.L.; Hantanasirisakul, K.; Lang, A.C.; Anasori, B.; Pinto, D.; Pivak, Y.; van Omme, J.T.; May, S.J.; Gogotsi, Y.; Taheri, M.L. Control of MXenes' electronic properties through termination and intercalation. *Nat. Commun.* **2019**, *10*, 522. [CrossRef]
145. Yang, L.; Dall'Agnese, C.; Dall'Agnese, Y.; Chen, G.; Gao, Y.; Sanehira, Y.; Jena, A.K.; Wang, X.-F.; Gogotsi, Y.; Miyasaka, T. Surface-Modified Metallic $Ti_3C_2T_x$ MXene as Electron Transport Layer for Planar Heterojunction Perovskite Solar Cells. *Adv. Funct. Mater.* **2019**, *29*, 1905694. [CrossRef]
146. Schultz, T.; Frey, N.C.; Hantanasirisakul, K.; Park, S.; May, S.J.; Shenoy, V.B.; Gogotsi, Y.; Koch, N. Surface Termination Dependent Work Function and Electronic Properties of $Ti_3C_2T_x$ MXene. *Chem. Mater.* **2019**, *31*, 6590–6597. [CrossRef]
147. Yun, T.; Kim, H.; Iqbal, A.; Cho, Y.S.; Lee, G.S.; Kim, M.-K.; Kim, S.J.; Kim, D.; Gogotsi, Y.; Kim, S.O.; et al. Electromagnetic Shielding of Monolayer MXene Assemblies. *Adv. Mater.* **2020**, *32*, 1906769. [CrossRef] [PubMed]
148. Yang, S.; Zhang, P.; Wang, F.; Ricciardulli, A.G.; Lohe, M.R.; Blom, P.W.M.; Feng, X. Fluoride-Free Synthesis of Two-Dimensional Titanium Carbide (MXene) Using a Binary Aqueous System. *Angew. Chem. Int. Ed.* **2018**, *57*, 15491–15495. [CrossRef] [PubMed]
149. Yang, Z.; Liu, A.; Wang, C.; Liu, F.; He, J.; Li, S.; Wang, J.; You, R.; Yan, X.; Sun, P.; et al. Improvement of Gas and Humidity Sensing Properties of Organ-like MXene by Alkaline Treatment. *ACS Sens.* **2019**, *4*, 1261–1269. [CrossRef]
150. Pandey, M.; Thygesen, K.S. Two-Dimensional MXenes as Catalysts for Electrochemical Hydrogen Evolution: A Computational Screening Study. *J. Phys. Chem. C* **2017**, *121*, 13593–13598. [CrossRef]
151. Chang, W.-C.; Cheng, S.-C.; Chiang, W.-H.; Liao, J.-L.; Ho, R.-M.; Hsiao, T.-C.; Tsai, D.-H. Quantifying Surface Area of Nanosheet Graphene Oxide Colloid Using a Gas-Phase Electrostatic Approach. *Anal. Chem.* **2017**, *89*, 12217–12222. [CrossRef] [PubMed]
152. Soliman, A.B.; Hassan, M.H.; Abugable, A.A.; Karakalos, S.G.; Alkordi, M.H. Post-Synthetic Immobilization of Ni Ions in a Porous-Organic Polymer-Graphene Composite for Non-Noble Metal Electrocatalytic Water Oxidation. *ChemCatChem* **2017**, *9*, 2946–2951. [CrossRef]
153. Meskher, H.; Mustansar, H.C.; Thakur, A.K.; Sathyamurthy, R.; Lynch, I.; Singh, P.; Han, T.K.; Saidur, R. Recent trends in carbon nanotube (CNT)-based biosensors for the fast and sensitive detection of human viruses: A critical review. *Nanoscale Adv.* **2023**, *5*, 992–1010. [CrossRef]
154. Ma, P.-C.; Siddiqui, N.A.; Marom, G.; Kim, J.-K. Dispersion and functionalization of carbon nanotubes for polymer-based nanocomposites: A review. *Compos. Part A Appl. Sci. Manuf.* **2010**, *41*, 1345–1367. [CrossRef]
155. Zhu, S.; Luo, F.; Li, J.; Zhu, B.; Wang, G.-X. Biocompatibility assessment of single-walled carbon nanotubes using Saccharomyces cerevisiae as a model organism. *J. Nanobiotechnol.* **2018**, *16*, 44. [CrossRef]
156. Molaei, M.J.; Younas, M.; Rezakazemi, M. A Comprehensive Review on Recent Advances in Two-Dimensional (2D) Hexagonal Boron Nitride. *ACS Appl. Electron. Mater.* **2021**, *3*, 5165–5187. [CrossRef]
157. Kim, J.; Han, J.; Seo, M.; Kang, S.; Kim, D.; Ihm, J. High-surface area ceramic-derived boron-nitride and its hydrogen uptake properties. *J. Mater. Chem. A* **2013**, *1*, 1014–1017. [CrossRef]
158. Chen, J.; Meng, H.; Tian, Y.; Yang, R.; Du, D.; Li, Z.; Qu, L.; Lin, Y. Recent advances in functionalized MnO_2 nanosheets for biosensing and biomedicine applications. *Nanoscale Horiz.* **2019**, *4*, 321–338. [CrossRef]
159. Mahmood, N.; De Castro, I.A.; Pramoda, K.; Khoshmanesh, K.; Bhargava, S.K.; Kalantar-Zadeh, K. Atomically thin two-dimensional metal oxide nanosheets and their heterostructures for energy storage. *Energy Storage Mater.* **2019**, *16*, 455–480. [CrossRef]
160. Jia, Z.; Wang, J.; Wang, Y.; Li, B.; Wang, B.; Qi, T.; Wang, X. Interfacial Synthesis of δ-MnO_2 Nano-sheets with a Large Surface Area and Their Application in Electrochemical Capacitors. *J. Mater. Sci. Technol.* **2016**, *32*, 147–152. [CrossRef]

161. Ikram, M.; Liu, L.; Liu, Y.; Ma, L.; Lv, H.; Ullah, M.; He, L.; Wu, H.; Wang, R.; Shi, K. Fabrication and characterization of a high-surface area MoS_2@WS_2 heterojunction for the ultra-sensitive NO_2 detection at room temperature. *J. Mater. Chem. A* **2019**, *7*, 14602–14612. [CrossRef]
162. El Beqqali, O.; Zorkani, I.; Rogemond, F.; Chermette, H.; Chaabane, R.B.; Gamoudi, M.; Guillaud, G. Electrical properties of molybdenum disulfide MoS_2. Experimental study and density functional calculation results. *Synth. Met.* **1997**, *90*, 165–172. [CrossRef]
163. Barua, S.; Dutta, H.S.; Gogoi, S.; Devi, R.; Khan, R. Nanostructured MoS_2-Based Advanced Biosensors: A Review. *ACS Appl. Nano Mater.* **2018**, *1*, 2–25. [CrossRef]
164. Zhang, J.; Kong, N.; Uzun, S.; Levitt, A.; Seyedin, S.; Lynch, P.A.; Qin, S.; Han, M.; Yang, W.; Liu, J.; et al. Scalable Manufacturing of Free-Standing, Strong $Ti_3C_2T_x$ MXene Films with Outstanding Conductivity. *Adv. Mater.* **2020**, *32*, 2001093. [CrossRef]
165. Ren, C.E.; Zhao, M.-Q.; Makaryan, T.; Halim, J.; Boota, M.; Kota, S.; Anasori, B.; Barsoum, M.W.; Gogotsi, Y. Porous Two-Dimensional Transition Metal Carbide (MXene) Flakes for High-Performance Li-Ion Storage. *ChemElectroChem* **2016**, *3*, 689–693. [CrossRef]
166. Chen, L.; Dai, X.; Feng, W.; Chen, Y. Biomedical Applications of MXenes: From Nanomedicine to Biomaterials. *Accounts Mater. Res.* **2022**, *3*, 785–798. [CrossRef]
167. Hang, G.; Wang, X.; Zhang, J.; Wei, Y.; He, S.; Wang, H.; Liu, Z. Review of MXene Nanosheet Composites for Flexible Pressure Sensors. *ACS Appl. Nano Mater.* **2022**, *5*, 14191–14208. [CrossRef]
168. Shahzad, F.; Iqbal, A.; Kim, H.; Koo, C.M. 2D Transition Metal Carbides (MXenes): Applications as an Electrically Conducting Material. *Adv. Mater.* **2020**, *32*, 2002159. [CrossRef] [PubMed]
169. Soomro, R.A.; Zhang, P.; Fan, B.; Wei, Y.; Xu, B. Progression in the Oxidation Stability of MXenes. *Nano-Micro Lett.* **2023**, *15*, 108. [CrossRef] [PubMed]
170. Liu, G.; Zou, J.; Tang, Q.; Yang, X.; Zhang, Y.; Zhang, Q.; Huang, W.; Chen, P.; Shao, J.; Dong, X. Surface Modified Ti_3C_2 MXene Nanosheets for Tumor Targeting Photothermal/Photodynamic/Chemo Synergistic Therapy. *ACS Appl. Mater. Interfaces* **2017**, *9*, 40077–40086. [CrossRef]
171. Lin, H.; Wang, Y.; Gao, S.; Chen, Y.; Shi, J. Theranostic 2D Tantalum Carbide (MXene). *Adv. Mater.* **2018**, *30*, 1703284. [CrossRef]
172. Basara, G.; Saeidi-Javash, M.; Ren, X.; Bahcecioglu, G.; Wyatt, B.C.; Anasori, B.; Zhang, Y.; Zorlutuna, P. Electrically conductive 3D printed Ti3C2Tx MXene-PEG composite constructs for cardiac tissue engineering. *Acta Biomater.* **2022**, *139*, 179–189. [CrossRef] [PubMed]
173. Han, X.; Huang, J.; Lin, H.; Wang, Z.; Li, P.; Chen, Y. 2D Ultrathin MXene-Based Drug-Delivery Nanoplatform for Synergistic Photothermal Ablation and Chemotherapy of Cancer. *Adv. Healthc. Mater.* **2018**, *7*, 1701394. [CrossRef] [PubMed]
174. Zong, L.; Wu, H.; Lin, H.; Chen, Y. A polyoxometalate-functionalized two-dimensional titanium carbide composite MXene for effective cancer theranostics. *Nano Res.* **2018**, *11*, 4149–4168. [CrossRef]
175. Dai, C.; Chen, Y.; Jing, X.; Xiang, L.; Yang, D.; Lin, H.; Liu, Z.; Han, X.; Wu, R. Two-Dimensional Tantalum Carbide (MXenes) Composite Nanosheets for Multiple Imaging-Guided Photothermal Tumor Ablation. *ACS Nano* **2017**, *11*, 12696–12712. [CrossRef]
176. Liu, J.; Jiang, X.; Zhang, R.; Zhang, Y.; Wu, L.; Lu, W.; Li, J.; Li, Y.; Zhang, H. MXene-Enabled Electrochemical Microfluidic Biosensor: Applications toward Multicomponent Continuous Monitoring in Whole Blood. *Adv. Funct. Mater.* **2019**, *29*, 1807326. [CrossRef]
177. Ren, X.; Huo, M.; Wang, M.; Lin, H.; Zhang, X.; Yin, J.; Chen, Y.; Chen, H. Highly Catalytic Niobium Carbide (MXene) Promotes Hematopoietic Recovery after Radiation by Free Radical Scavenging. *ACS Nano* **2019**, *13*, 6438–6454. [CrossRef] [PubMed]
178. Lim, G.P.; Soon, C.F.; Ma, N.L.; Morsin, M.; Nayan, N.; Ahmad, M.K.; Tee, K.S. Cytotoxicity of MXene-based nanomaterials for biomedical applications: A mini review. *Environ. Res.* **2021**, *201*, 111592. [CrossRef] [PubMed]
179. Imani Yengejeh, S.; Kazemi, S.A.; Wen, W.; Wang, Y. Oxygen-terminated M4X3 MXenes with superior mechanical strength. *Mech. Mater.* **2021**, *160*, 103957. [CrossRef]
180. Li, Q.-F.; Chen, X.; Wang, H.; Liu, M.; Peng, H.-L. Pt/MXene-Based Flexible Wearable Non-Enzymatic Electrochemical Sensor for Continuous Glucose Detection in Sweat. *ACS Appl. Mater. Interfaces* **2023**, *15*, 13290–13298. [CrossRef]
181. Feng, L.; Qin, W.; Wang, Y.; Gu, C.; Li, X.; Chen, J.; Chen, J.; Qiao, H.; Yang, M.; Tian, Z.; et al. $Ti_3C_2T_x$ MXene/Graphene/AuNPs 3D porous composites for high sensitivity and fast response glucose biosensing. *Microchem. J.* **2023**, *184*, 108142. [CrossRef]
182. Gilnezhad, J.; Firoozbakhtian, A.; Hosseini, M.; Adel, S.; Xu, G.; Ganjali, M.R. An enzyme-free Ti_3C_2/Ni/Sm-LDH-based screen-printed-electrode for real-time sweat detection of glucose. *Anal. Chim. Acta* **2023**, *1250*, 340981. [CrossRef]
183. Li, M.; Wang, L.; Liu, R.; Li, J.; Zhang, Q.; Shi, G.; Li, Y.; Hou, C.; Wang, H. A highly integrated sensing paper for wearable electrochemical sweat analysis. *Biosens. Bioelectron.* **2021**, *174*, 112828. [CrossRef]
184. Lei, Y.; Zhao, W.; Zhang, Y.; Jiang, Q.; He, J.-H.; Baeumner, A.J.; Wolfbeis, O.S.; Wang, Z.L.; Salama, K.N.; Alshareef, H.N. A MXene-Based Wearable Biosensor System for High-Performance In Vitro Perspiration Analysis. *Small* **2019**, *15*, 1901190. [CrossRef]
185. Magesh, V.; Sundramoorthy, A.K.; Ganapathy, D.; Atchudan, R.; Arya, S.; Alshgari, R.A.; Aljuwayid, A.M. Palladium Hydroxide (Pearlman’s Catalyst) Doped MXene ($Ti_3C_2T_x$) Composite Modified Electrode for Selective Detection of Nicotine in Human Sweat. *Biosensors* **2023**, *13*, 54. [CrossRef]

186. Myndrul, V.; Coy, E.; Babayevska, N.; Zahorodna, V.; Balitskyi, V.; Baginskiy, I.; Gogotsi, O.; Bechelany, M.; Giardi, M.T.; Iatsunskyi, I. MXene nanoflakes decorating ZnO tetrapods for enhanced performance of skin-attachable stretchable enzymatic electrochemical glucose sensor. *Biosens. Bioelectron.* **2022**, *207*, 114141. [CrossRef]
187. Hui, X.; Sharifuzzaman, M.; Sharma, S.; Xuan, X.; Zhang, S.; Ko, S.G.; Yoon, S.H.; Park, J.Y. High-Performance Flexible Electrochemical Heavy Metal Sensor Based on Layer-by-Layer Assembly of $Ti_3C_2T_x$/MWNTs Nanocomposites for Noninvasive Detection of Copper and Zinc Ions in Human Biofluids. *ACS Appl. Mater. Interfaces* **2020**, *12*, 48928–48937. [CrossRef]
188. Nah, J.S.; Barman, S.C.; Zahed, M.A.; Sharifuzzaman, M.; Yoon, H.; Park, C.; Yoon, S.; Zhang, S.; Park, J.Y. A wearable microfluidics-integrated impedimetric immunosensor based on $Ti_3C_2T_x$ MXene incorporated laser-burned graphene for noninvasive sweat cortisol detection. *Sens. Actuators B Chem.* **2021**, *329*, 129206. [CrossRef]
189. Zhi, C.; Shi, S.; Zhang, S.; Si, Y.; Yang, J.; Meng, S.; Fei, B.; Hu, J. Bioinspired All-Fibrous Directional Moisture-Wicking Electronic Skins for Biomechanical Energy Harvesting and All-Range Health Sensing. *Nano-Micro Lett.* **2023**, *15*, 60. [CrossRef]
190. Zhang, Y.; Wang, Z.; Liu, X.; Liu, Y.; Cheng, Y.; Cui, D.; Chen, F.; Cao, W. A MXene/MoS_2 heterostructure based biosensor for accurate sweat ascorbic acid detection. *FlatChem* **2023**, *39*, 100503. [CrossRef]
191. Qiao, Y.; Liu, X.; Jia, Z.; Zhang, P.; Gao, L.; Liu, B.; Qiao, L.; Zhang, L. In Situ Growth Intercalation Structure MXene@Anatase/Rutile TiO_2 Ternary Heterojunction with Excellent Phosphoprotein Detection in Sweat. *Biosensors* **2022**, *12*, 865. [CrossRef]
192. Chen, L.; Chen, F.; Liu, G.; Lin, H.; Bao, Y.; Han, D.; Wang, W.; Ma, Y.; Zhang, B.; Niu, L. Superhydrophobic Functionalized Ti3C2Tx MXene-Based Skin-Attachable and Wearable Electrochemical pH Sensor for Real-Time Sweat Detection. *Anal. Chem.* **2022**, *94*, 7319–7328. [CrossRef] [PubMed]
193. Ates, H.C.; Nguyen, P.Q.; Gonzalez-Macia, L.; Morales-Narváez, E.; Güder, F.; Collins, J.J.; Dincer, C. End-to-end design of wearable sensors. *Nat. Rev. Mater.* **2022**, *7*, 887–907. [CrossRef] [PubMed]
194. Shuck, C.E.; Sarycheva, A.; Anayee, M.; Levitt, A.; Zhu, Y.; Uzun, S.; Balitskiy, V.; Zahorodna, V.; Gogotsi, O.; Gogotsi, Y. Scalable Synthesis of $Ti_3C_2T_x$ MXene. *Adv. Eng. Mater.* **2020**, *22*, 1901241. [CrossRef]
195. Chen, N.; Duan, Z.; Cai, W.; Wang, Y.; Pu, B.; Huang, H.; Xie, Y.; Tang, Q.; Zhang, H.; Yang, W. Supercritical etching method for the large-scale manufacturing of MXenes. *Nano Energy* **2023**, *107*, 108147. [CrossRef]
196. Luo, Y.; Que, W.; Bin, X.; Xia, C.; Kong, B.; Gao, B.; Kong, L.B. Flexible MXene-Based Composite Films: Synthesis, Modification, and Applications as Electrodes of Supercapacitors. *Small* **2022**, *18*, 2201290. [CrossRef]
197. Huang, H.; Jiang, R.; Feng, Y.; Ouyang, H.; Zhou, N.; Zhang, X.; Wei, Y. Recent development and prospects of surface modification and biomedical applications of MXenes. *Nanoscale* **2020**, *12*, 1325–1338. [CrossRef] [PubMed]

Disclaimer/Publisher's Note: The statements, opinions and data contained in all publications are solely those of the individual author(s) and contributor(s) and not of MDPI and/or the editor(s). MDPI and/or the editor(s) disclaim responsibility for any injury to people or property resulting from any ideas, methods, instructions or products referred to in the content.